Stomatin modulates adipocyte differentiation through ERK pathway and regulates lipid droplet growth and function

Shao-Chin Wu
National Yang-Ming University/Biophotonics https://orcid.org/0000-0002-1960-1581
Yuan-Ming Lio
National Yang-Ming University/Microbiology and Immunology
Jui-Hao Lee
National Yang-Ming University/Taiwan International Graduate Program in Molecular Medicine
Chin-Yau Chen
National Yang-Ming University Hospital
Tung-Wei Chen
National Yang-Ming University
Hong-Wen Liu
National Yang-Ming University
Wei-Nan Lian
National Yang-Ming University
Wei-Ju Lin
National Yang-Ming University/Cancer Progression Research Center
Chih-Yung Yang
Taipei City Hospital
Chien-Yi Tung
National Yang-Ming University/Cancer Progression Research Center
Chi-Hung Lin (linch@ym.edu.tw)
National Yang-Ming University/Biophotonics

Article

Keywords: Stomatin, adipocyte differentiation, ERK pathway, lipid droplet growth and function

Posted Date: November 10th, 2020

DOI: https://doi.org/10.21203/rs.3.rs-94915/v1

Version of Record: A version of this preprint was published at Nature Communications on July 19th, 2022. See the published version at https://doi.org/10.1038/s41467-022-31825-z.

Stomatin modulates adipocyte differentiation through ERK pathway and regulates lipid droplet growth and function

Shao-Chin Wu[1], Yuan-Ming Lio[2], Jui-Hao Lee[3], Chin-Yau Chen[4], Tung-Wei Chen[1], Hong-Wen Liu[5], Wei Nan Lian[2], Wei-Ju Lin[6] Chih-Yung Yang[7], Chien-Yi Tung[6#], Chi-Hung Lin[1,2,6,8*]

1. Institute of Biophotonics, National Yang-Ming University, Taipei, Taiwan
2. Institute of Microbiology and Immunology, National Yang-Ming University, Taipei, Taiwan
3. Taiwan International Graduate Program in Molecular Medicine, National Yang-Ming University and Academia Sinica, Taipei, Taiwan
4. National Yang-Ming University Hospital, Yilan, Taiwan
5. Chong Hin Loon Memorial Cancer and Biotherapy Research Center, Taipei, Taiwan
6. Cancer Progression Research Center, National Yang-Ming University, Taipei, Taiwan
7. Department of Education and Research, Taipei City Hospital, Taipei, Taiwan
8. Department of Biological Science and Technology, National Chiao-Tung University, Hsinchu, Taiwan

***Correspondence**

Chi-Hung Lin, MD, ph.D.

Institute of Biophotonics, National Yang-Ming University, Taipei, Taiwan
Institute of Microbiology and Immunology, National Yang-Ming University, Taipei, Taiwan
Cancer Progression Research Center, National Yang-Ming University, Taipei, Taiwan
Department of Biological Science and Technology, National Chiao-Tung University, Hsinchu, Taiwan
No.155, Sec.2, Linong Street, Taipei, 112 Taiwan (ROC)
Telephone: +886-2-28267000#5613
E-mail: linch@ym.edu.tw

#Co-correspondence

Chien-Yi Tung, ph.D.

Cancer Progression Research Center, National Yang-Ming University, Taipei, Taiwan
No.155, Sec.2, Linong Street, Taipei, 112 Taiwan (ROC)
Telephone: +886-2-28267000#5678

E-mail: E-mail: Cytung@ym.edu.tw

Abstract

Controlling fatty acid uptake, lipid production and storage, and metabolism of lipid droplets (LDs), are closely related to lipid homeostasis, adipocyte hypertrophy and obesity. We report here that stomatin, a major constituent of the lipid raft, participate in adipogenesis and lipogenesis by preferentially recruiting effectors, such as perilipin for LD fusion or transporters for fatty acid uptake. Adipocyte-like cells having increased stomatin expressions exhibit higher levels of fatty acid uptake and LD growth or enlargements. Moreover, transgenic mice fed with a high-fat diet showed increased stomatin expression that facilitated progression of obesity and caused insulin resistance and hepatic impairments. Conversely, inhibitions of stomatin by gene knockdown or pharmacological treatments could block not only LD growth but also adipogenic differentiation through downregulation of PPARγ pathway. Effects of stomatin on PPARγ involved ERK signaling; however, an alternate pathway also exist. Amongst various anti-obesity measures, stomatin serves as another potential therapeutic target.

Introduction

Stomatin is an ancient, widely expressed, oligomeric, monotopic integral membrane protein that is associated with cholesterol-rich membrane microdomains/lipid rafts. Besides being a major component of the lipid raft, functions of stomatin are largely unclear. The gene was first identified as the causal factor of Overhydrated Hereditary Stomatocytosis (OHSt) disease, and was therefore named “stomatin” [1, 2]. However, stomatin knockout mouse was viable and did not show stomatocytosis [3]. Human stomatin is ubiquitously expressed; high expressions are noted in adipose tissues, bone marrow and placenta (Supplemental Fig. 1). In placenta, stomatin plays an important role in trophoblast differentiation [4]; and in bone, stomatin promotes osteoclastogenesis [5]. At the cell level, stomatin is associated with the plasma membrane and cytoplasmic vesicles, such as endosomes [6], lipid droplets (LDs) [7], and specialized endosomes/granules in hematopoietic cells [8]. We have previously reported that stomatin, with its unique molecular topology, promoted cell-cell fusion by forming molecular assembly that recruited fusogenic protein to the appositional plasma membranes [5]. In addition to the regulations of fusion events, stomatin can also interact with various plasma membrane proteins residing within lipid raft and modulate

their activities. For examples, stomatin can regulate the transport activities of Anion Exchanger 1 (AE1) [9], glucose transporter (GLUT1) [10] and water channel aquaporin-1 (AQP1) [11], or activity of acid-sensing ion channel (ASIC) family[12, 13, 14]. Whether such regulations are mediated by stomatin's scaffolding effects that change the biophysical properties of the lipid rafts or by direct protein-protein interactions between stomatin and the effector molecules, are currently unknown. It is also unclear if and how stomatin is involved in signal transduction which is initiated by complex protein–protein interactions between ligands, receptors and signaling molecules that may occur in the vicinity of lipid rafts. It has been speculated that the size and composition of lipid rafts could change in response to intra- or extracellular stimuli; such changes might favor specific protein–protein interactions and activate corresponding signaling cascades. In this study, we addressed the roles of stomatin in adipocyte differentiation and functions, focusing on intracellular vesicular fusion among LDs, fatty acid uptake and their associated signal transduction.

Obesity, resulting from a positive energy balance between energy harvest and energy expenditure [15, 16], is a prevalent global healthcare problem that continues to increase in countries around the world [17]. Obesity is characterized by increased adipose tissue mass that has been associated with a strong predisposition towards metabolic diseases such as diabetes, cardiovascular diseases, non-alcoholic fatty liver diseases and some cancers [18, 19, 20]. The expansion of adipose depots, especially the white adipose tissues, are characterized either by the increase in adipocyte size (hypertrophy) or by the formation of new adipocytes from precursor differentiation in the process of adipogenesis (hyperplasia). Genetic and behavioral attributors both contribute to obesity-related energy imbalance [21, 22]. In the presence of excessive energy, mature adipocytes increase in cell size and undergo cellular hypertrophy to store the surplus fat [23].

Hypertrophic adipose morphology is positively associated with insulin resistance, diabetes and cardiovascular disease. The hypertrophic adipocytes are ultimately responsible for dysfunction of lipid homeostasis, along with other pathological consequences [24]. Hypertrophic adipocytes are characterized by excessive growth of LDs; the resulting unilocular LD may occupy more than 90% of the cell volume[25]. The

growth of LDs is achieved by incorporation of triacylglyceride (TG) that is synthesized either locally on the surface of LDs [26], or obtained from the endoplasmic reticulum [27]. Since fatty acid (FA) is the primary energy source assimilated by adipocytes during lipogenesis, measurements of FA uptake are indicative of LD growth [28, 29]. LDs can also grow via fusion of small LDs [30]. Previous studies have shown that several surface proteins of LDs were involved in controlling the LD size in adipocytes. For examples, Perilipin (Plin1), a member of PAT family proteins highly expressed in adipocytes, could regulate the lipolysis functions [31, 32]. The cell death-inducing DNA fragmentation factor alpha (DFFA)-like effector (CIDE) family proteins, Cidea, and Fsp27/Cidec, also functioned as LDs size regulators [33, 34]. Cooperative interactions of Plin1 and Fsp27 enhanced lipid transfer and LD growth [35].

Adipogenesis is the process by which adipose tissues expand through hyperplastic growth and differentiation. The formation of new adipocytes from precursor cells enhance the capacity of energy storage. Adipogenesis is characterized by expressions of C/EBPβ and C/EBPδ, followed by C/EBPα and PPARγ. The master transcription regulator PPARγ controls a variety of genes involved in adipogenesis [36, 37]. Previous studies have shown that activation of MAPK/ERK pathway (also known as the Ras-Raf-MEK-ERK pathway) could down-regulate transcriptional activity of PPARγ [38, 39] and inhibit adipocyte differentiation.

Approaches aimed at increasing adipogenesis over adipocyte hypertrophy are now regarded as a means to treat metabolic diseases. Notably, adipocyte expansion through adipogenesis could mitigate the negative metabolic effects of obesity, although the mechanisms and regulators are not fully understood [40]. This study addressed cell biology and signaling pathways of adipocyte-like cells affected by stomatin and provide insight into the control of adipogenesis and hypertrophic adipocytes related to obesity.

Results

Expressions of Stomatin increased during adipogenic differentiation

A cell model for adipogenic differentiation was established [41]. Treating murine 3T3-L1 fibroblasts with MDI cocktail for three days (day0 ~ day3), followed by insulin treatment (day3 ~ day7), rendered the cells to differentiate into adipocytes-like cells, as evidenced by lipid accumulation visualized and quantified by Oil Red O staining (Fig. 1A). Western blotting assays demonstrated that the expression of stomatin, as well as major adipogenic proteins, such as PPARγ, C/EBPα, and Perilipin, progressively increased during adipogenesis (Fig. 1B). After 7-day differentiation, mature adipocytes containing large lipid droplets (LD) were noted under DIC microscopy and stained positive with Oil Red O. Immunofluorescence staining revealed subcellular distributions of stomatin mainly on the vesicular membranes of LDs, colocalized with perilipin proteins (Fig. 1C).

High expressions of Stomatin enhanced LD growth

To understand the roles of stomatin in adipogenic differentiation, we over-expressed human stomatin gene (hSTOM) in murine 3T3-L1 cells. After chemically induced differentiation, we found that the levels of lipid accumulation and adipogenic proteins were very similar in cells having excessive exogenous stomatin proteins, compared to the control (Fig. 2A-B). However, when measuring the size of individual LDs, we noticed that there were more large-sized LDs in cells expressing hSTOM than the control (Fig. 2C), indicating that stomatin were involved in LD growth, or large LD formation. Such dynamics of LDs could result from either fusion of small LDs into a large one (exemplified by Supplemental Video 1 that captures the sequence of a LD-LD fusion event), or from exchanges of lipid content between interacting LDs.

Since small LD vesicles were not discernible under light microscopy, we employed fluorescence recovery after photobleaching (FRAP) experiments to investigate LD activities. As shown in Fig. 2E, photobleaching the fluorescent lipid content of a LD resulted in a fast recovery of fluorescence, reaching half of the original intensity in 15 min in cells over-expressing stomatin compared to a very slow recovery, reaching less

than 8% of original intensity in 15 min, in the control cells. These results indicate an active role of stomatin in facilitating dynamic interactions between LDs.

Highly abundant Stomatin facilitates fatty acid uptake both in vitro and in vivo

The process of lipid biogenesis, or lipogenesis, starts with either de novo synthesis, or fatty acid uptake from extracellular environment using various fatty acid transporters [42]. In the experimental assay shown in Fig. 2F, fluorescently labeled palmitic acid analogs, BODIPY-C16, when added to the culture medium, were internalized into the cells and quantified continuously using an ELISA reader. Cells having high abundance of stomatin exhibited more and faster fatty acid uptake compared to the control. Moreover, *in vivo* fatty acid uptake experiments were performed in STOM transgenic (STOM Tg) mice. BSA-emulsified BODIPY-C16 were injected into tail vein; after 15 min, there were much more fluorescence signals found in the adipose tissues of STOM Tg than the control mice (Fig. 3F).

High expressions of Stomatin caused obesity in mice fed with high-fat diet

We generated STOM transgenic (STOM Tg) mice by engineering human stomatin gene into the animal. These mice contained high amount of hSTOM proteins in subcutaneous white adipose tissues, distributed mainly on the surfaces of white adipocytes (Fig. 3A-B). STOM Tg and the control wild-type (WT) mice were fed either regular chow diet (CD), or high-fat diet (HFD) beginning at 3 weeks of age; the mice were weighed every week. We noticed that body weight gains were about the same comparing STOM Tg with WT mice fed with CD. When fed with HFD, however, mice having up-regulated STOM gene gained more weights more rapidly than their WT littermates (Fig. 3C-D). After 20 weeks, body weights of HFD-fed STOM Tg were at least 20% higher than WT. Whole-body composition measurements showed that the increase of fat was more significant than increases of lean, free fluid or total water (Fig. 3E).

HFD-fed STOM Tg mice exhibited adipocyte hypertrophy, impaired metabolisms and hepatic dysfunctions

After 20-week HFD feeding, mice having up-regulated STOM gene showed significant increase in subcutaneous adipose tissue (SAT) and brown adipose tissue (BAT) than

WT, whereas mass of visceral adipose tissue (VAT) were about the same (Fig. 4A). Adipocytes from SAT of HFD-fed STOM Tg mice appeared hypertrophic; they were larger in size than those of WT littermates by histogram analyses (Fig. 4B). In addition, Western blotting of 3T3-L1 adipocyte-like cells showed that enzymes for lipolysis, including perilipin and hormone-sensitive lipase (HSL) and its various serine-phosphorylated forms, were similar in cells having over-expressed hSTOM and control cells (Supplemental Fig. 2A), indicating that the observed adipocyte hypertrophy caused by stomatin was not due to impaired triglyceride metabolism.

The observed obesity was not a result of altered energy expenditure or energy substrate selection, as evidenced by similar respiratory exchange rates comparing HFD-fed STOM Tg mice and their littermate controls (Supplemental Fig. 2B). The calculated heat production during the light-dark cycle showed that HFD-fed STOM Tg mice had only slightly higher heat production which was too little to influence obesity progression (Supplemental Fig. 2C).

Biochemical analysis after 20-week HFD feeding showed that total cholesterol (TCHO) of HFD-fed STOM Tg were slightly higher than the control, but triglycerides (TG) levels were the same (Supplemental Fig. 2D). Interestingly, although fasting blood glucose were similar between the groups, plasma insulin and insulin resistance measured by HOMA-IR experiments, and glucose tolerance measured by intraperitoneal glucose tolerance test (IPTGG) were much higher and intolerable in STOM Tg than WT mice (Fig. 4C). These results indicated that HFD-fed, STOM Tg aggravated glucose homeostasis by enhancing insulin resistance.

Obesity is usually correlated with ectopic fat accumulation in the liver. Indeed, HFD-fed STOM Tg possessed not only larger liver mass (hepatomegaly), but also exhibited phenotypes of macro- and microvesicular steatosis. The observed hepatic steatosis appeared to affect liver functions, as evidenced by elevated levels of plasma GPT and GOP in HFD-fed STOM Tg mice (Fig. 4D).

Knockdown of STOM inhibited adipogenesis and LD growth

Knockdown of STOM expression was done by short hairpin RNA (shRNA) method. Two shRNAs designed to target different sites of murine stomatin were separately packaged into lentiviral particles and introduced into 3T3-L1cells, resulting in shSTOM-1 and shSTOM-2 cells. Both shRNAs could effectively down-regulate stomatin expressions. Knocking-down STOM expression inhibited not only adipogenesis, evidenced by lack of lipid accumulation (Fig. 5A) and inhibitions of genes involved in adipocytic differentiation, such as PPARγ and C/EBPα (Fig. 5B). Knockdown of STOM also inhibited LD growth. As shown by Fig. 5C, histogram analyses of LD sizes revealed more small-LD and fewer large-LD following STOM knockdown.

Differential expressions of shSTOM-1 and control cells were analyzed after induction of adipogenic differentiation for seven days by the microarray method. A total of 1478 annotated coding genes were identified from the transcriptomes by a stringent threshold of P value < 0.05 and FDR P value < 0.001. Among them, 379 transcripts were of significant difference between Stom-deficient and control cells (fold change $\geq$ 3, or $\leq$ -3); 185 of them were up-regulated and 194 down-regulated by inhibition of stomatin expression (Supplemental Fig. 3A). The global view of these genes was constructed by hierarchical clustering to characterize changes across six samples (Supplemental Fig. 3B). These genes were mapped onto 128 Wikipathways using Transcriptome Analysis Console (TAC). As the top-tanking enriched pathways shown (Fig. 5D), adipogenesis genes were the most profoundly inhibited gene groups, followed by PPAR signaling pathway. In the “adipogenesis genes” pathway, 12 genes involved in this pathway showed significant changes; 9 of them (75%) were down-regulated and 3 (25%) were up-regulated (Fig. 5E). To further validate the results, we performed qPCR experiments for *Pparg* and *Cebpa* genes and confirmed transcriptomic findings (Fig. 5F).

Somatin inhibitor OB-1 affected adipogenic differentiation and inhibited LD growth

By inhibiting self-association, OB-1 is an effective inhibitor of stomatin-mediated functions [43]. LD_{50} for OB-1 in 3T3-L1 cells was first determined (Fig. 6A). Drug

treatments using 25 μM OB-1, while maintaining good cell viability, inhibited adipogenic differentiation in a dose-dependent manner as evidenced by decreased lipid accumulation (Fig. 6B). Treating 3T3-L1 cells during adipocytic differentiation with OB-1 also inhibited LD growth; histogram analyses of LD sizes were applied to quantify the increase of small LDs and decrease of large LDs (Fig. 6C).

Stomatin modulated adipocyte differentiation through ERK pathway

Inhibitions of stomatin by either shRNA (Fig. 5A) or OB-1 (Fig. 6B) could effectively block lipid accumulation by adipocytic 3T3-L1 cells. Using Western blotting assays, we analyzed their effects on other adipogenesis-related genes and signaling pathways (Fig. 7). Both stomatin-deficient shSTOM-1 and shSTOM-2 cells exhibited decreased PPARγ protein. While the Akt pathway was not affected by STOM knockdown, the ERK pathway appeared activated as evidenced by the increased level of phosphorylated ERK (*arrow*, Fig. 7A). OB-1 treatment also caused increase of phospho-ERK (Fig. 7D).

Two early adipogenesis genes, C/EBPβ and C/EBPδ, are upstream of PPARγ regulation. After induction of adipogenic differentiation, C/EBPβ and C/EBPδ, exhibited a transient increase in the first three days, followed by a gradual decrease from day 3 to day 7 (Fig. 7B and 7C, respectively). Knockdown of stomatin had little effect on the protein levels and degrees of C/EBPβ phosphorylation (data not shown); in contrast, inhibition of stomatin was able to maintain C/EBPδ expression at much higher level than the control (Fig. 7B-C).

Since activation of ERK pathway has been shown to inhibit PPARγ [44], we examined whether stomatin positively regulated PPARγ regulation via inhibition of pERK (*red arrows*, Fig. 8). To this end, we treated shSTOM-1 cells with U0126, a highly selective inhibitor for ERK, under the notion that U0126 might mitigate the stomatin-knockdown effect of pERK activation. However, we found that U0126 treatment could not reverse the lipogenesis-deficit phenotype of hSTOM-1 cells (Fig. 7E). In contrast, treating hSTOM-1 cells with troglitazone (TGZ), a PPARγ agonist, was able to partially rescue lipogenesis-deficit of hSTOM-1 cells; and interestingly, dual treatments of U0126 and TGZ were noted to further recover lipid accumulation (Fig. 7F). These results suggest

the presence of a currently unknown mechanism for stomatin to positively regulate PPARγ and activate adipogenesis (*black arrows*, Fig. 8); this unknown pathway may work synergistically with the ERK pathway.

Discussion

We propose a working model for the roles of stomatin in adipogenic differentiation and lipogenesis (Fig. 8). Along the differentiation process from undifferentiated progenitor cells to immature adipocytes then to mature adipocyte, expression of stomatin progressively increase. C/EBPβ and C/EBPδ exhibits a transient increase during the early phase, while C/EBPα in the later phase. The various adipogenic genes and signaling processes seem to converge onto the PPARγ pathway, which is considered one of the master regulators of adipocyte differentiation [37]. We report a novel finding that knockdown of stomatin was able to activate ERK signaling as evidenced by the increase of pERK. Since pERK is a well-known negative regulator of PPARγ we wonder if the promoting effect of stomatin on PPARγ and the downstream adipogenic phenotype is mediated through downregulation of pERK (*red arrows*, Fig. 8, see also [44]). Our results (Fig. 7E-F), however, did not support this notion. Unlike activation of PPARγ, activation of ERK pathway alone did not rescue the lipogenesis deficit caused by stomatin knockdown. This suggests the presence of another currently unknown pathway (*black arrow*, Fig. 8) that may work synergistically with ERK pathway to activate PPARγ and by doing so promote adipogenesis and lipogenesis.

What signaling events are affected by stomatin which serves a major role as a component of lipid rafts? Through transcriptome and pathway analyses, we identified MAPK signaling as a potential pathway affected by stomatin (Fig. 5D-E and supplemental Fig. 3). In the case of adipocyte differentiation, EGFR is one of the upstream receptor tyrosine kinases (RTKs) for MAPK signaling. RTKs control many fundamental cell behaviors by activating a series of downstream signaling pathways including RAS-RAF-MEK-ERK pathway or AKT-PI3K-mTOR pathway [45, 46]. We found that the RAS-RAF-MEK-ERK pathway is involved in stomatin-mediated adipogenic differentiation (Fig. 7A). Also, EGFR metabolism is highly regulated by lipid-raft mediated internalization, recycling and degradation[47, 48, 49, 50]. Increased expression of stomatin, for example, caused a reduction in EGFR on the plasma membrane

313 (unpublished data), resulting in reduced ERK activity which is necessary for adipocyte
314 differentiation [45].
315
316 Besides participating in modulation of signaling during adipogenic differentiation,
317 stomatin also plays a crucial role in LD growth characterized by vesicle enlargement
318 and transformation from multilocular LDs to unilocular LDs typically seen in adipose
319 tissues. LD is a universal cellular organelle that responds to lipid storage. It is believed
320 to be generated from the endoplasmic reticulum (ER) [51] and can enlarge through the
321 incorporation of lipid from the ER [52], the local synthesis of triacylglycerols (TAGs) [26,
322 53], and the fusion of multiple lipid droplets [54]. Stomatin, as a LD-associated protein [7]
323 and a major lipid raft component, could play multiple roles in growth of LD. First,
324 stomatin if present in high abundance could promote formation of potential fusion
325 pores that leads to LD fusion[4, 5]. Second, stomatin could recruit fusion facilitators to
326 LD-LD contact site (LDCS), and by doing so regulate LD-fusion and growth. Third,
327 stomatin could help generate passage tunnels that allow lipid exchange among
328 contacted LDs [35, 55]. Due either to illumination toxicity to the cell or the fact that the
329 majority LD undergoing fusion were of submicron-sized, direct imaging of fusion
330 between micron-sized LD was hard to achieve under light microscopy. We therefore
331 employed FRAP experiments to address the third mechanism. Lipids in the smaller
332 LDs of the contacted pair are transferred to the larger LDs, owing to the internal
333 pressure difference, thus resulting in the fusion and growth of LDs.
334
335 For the aforementioned second mechanism, we have previously reported that
336 stomatin works as an "enhancer" on the plasma membrane to increase the
337 effectiveness of molecular machinery for membranes fusion[4, 5]. Within a lipid raft, for
338 example, stomatin can restrict existing fusogenic effectors to the sites of membrane-
339 membrane contact and enhance their interactions. The same mechanism may apply
340 to intracellular inter-vesicular fusions. Locally enriched stomatin and perilipin can
341 recruit cell death-inducing DFF45-like effector (CIDE) family proteins to LDCS [35]. As
342 CIDE family proteins are crucial regulators of LD-fusion [56], the “fencing” mechanism
343 by stomatin can promote fusion pore expansion at LDCS, resulting in LD fusion and
344 growth.
345

The ability of adipocyte to uptake fatty acid of superfluous lipids from the extracellular environment is impacted by their physiological functions in energy homeostasis. The amount and rate of fatty acid uptake were noted to increase in the presence of high level stomatin both *in vitro* and *in vivo*. Although some fatty acids can cross plasma membrane by passive diffusion [57], most fatty acid uptake is mediated by membrane-associated transporters; many of them reside and function in the lipid rafts. When bound to long-chain fatty acid (LCFAs), FAT/CD36 may partition into lipid rafts to accelerate the translocation of LCFAs [28, 58]. In lipid rafts, stomatin can function as an anchor or organizer for these cholesterol-rich membrane domains. Stomatin can also modulate the function of effector residing within lipid rafts. For example, stomatin can regulate several ion channels activities[59, 60] and glucose transport GLUT1 functions [10]. In a more general sense, stomatin can capture or trap the lateral diffusion of proteins within the lipid raft or affect the interaction between ligand and receptors, and by doing so, regulate the downstream signaling transduction.

Adipose tissues play a central role in regulating energy storage to protect other tissues, such as the muscle and the liver, from the harmful effects of superfluous circulating free fatty acid. So, fatty acid uptake and LD growth are crucial in controlling lipid storage and obesity development. We demonstrated here that high levels of stomatin, combined with chronic energy surplus, may lead to a hypertrophy phenotype of adipocytes (the HFD-fed STOM Tg mice). The resulting limitation in fat storage capacity then cause local and systemic metabolism disorders [61]. In a broader sense, stomatin is involved in regulating various aspects of lipid homeostasis, including adipocyte differentiation, lipid production, lipid storage, lipolysis and lipid secretion. The finding that stomatin regulates fatty acid uptake and LD growth may provide new opportunities for correcting whole-body energy disorders or energy surplus-induced obesity by modulating the molecular events associated with stomatin.

Methods

Cell Culture and induction of adipogenic differentiation

3T3-LI murine fibroblasts, purchased from Bioresource Collection and Research Center (no.60159; BCRC, Hsinchu, Taiwan), were maintained in high-glucose Dulbecco's modified Eagle's medium (DMEM) supplemented with 10 % bovine calf *serum* and 1% sodium pyruvate. To induce differentiation into adipocyte-like cells, 3T3-LI cells were first grown to confluence. Two days after reaching confluence, the medium was replaced with DMEM supplemented with 10 % fetal bovine serum (FBS) containing MDI cocktail, including 0.5 mM IBMX, 0.25 μM dexamethasone and 10 μg/ml bovine insulin. After 72 hours, the medium was replaced with DMEM supplemented with 10 % FBS and 10 μg/ ml bovine insulin. The medium was refreshed every other day. Human embryonic kidney (HEK) 293T cells were cultured in DMEM supplemented with 10 % FBS.

Lentivirus production and transduction

Lenti-Vector pLAS2W.puro, shRNA for *Stom* vectors (shSTOM-1: clone number TRCN0000112911 and shSTOM-2: clone number TRCN 0000112912) and packaging plasmids pCMV delta R8.91 and PMD.G were obtained from National RNAi Core Facility Platform (Acadamic Sinica, Taiwan). RFP, hSTOM-RFP and hSTOM-flag (hSF) were amplified from expression plasmids and cloned into the lenti-Vector. HEK-293T cells were co-transfected with lentivector and packaging plasmids using NTR II Non-liposome transfection reagent II (T-Pro-Biotechnology, Taiwan). The supernatants containing lentivirus were harvested after 24- and 48-hr and centrifuged at 1,250 rpm for 5 min to exclude any remaining HEK-293T packaging cells. Subsequently, cells were transduced with the lentivirus-containing supernatants for 24 hrs, followed by 3 μg/mL puromycin selection for 3 days.

Quantifications of lipid accumulation

Oil Red O stock solution was prepared by dissolving 0.35g Oil Red O (no. O0625, Sigma Aldrich) in 100ml pure isopropanol. Cells were fixed with 3.7% formaldehyde for 1 hr at room temperature, followed by two times wash, then dried entirely using a hairdryer. Post-fixed cells were stained with Oil Red O, diluted in distilled water (6:4)

for 1 hr at room temperature, further washed four times with distilled water. The stained dyes in lipid droplets were extracted with pure isopropanol and absorbance at 490 nm (OD 490) was measured.

Western blot analysis

Cultured cells were washed twice with cold PBS, then lysed using RIPA lysis buffer supplemented with cOmplete™ (EDTA-free Protease Inhibitor Cocktail) and PhosSTOP™ (both from Sigma Aldrich). The amount of total extracted proteins was quantified using Pierce 660nm protein assay reagent (Thermo Fisher Scientific ™). The protein lysates were separated by SDS-PAGE, then transferred onto PVDF membranes. The membranes were blocked with 5% bovine serum albumin (BSA) in TBS-T (Tris-buffer saline supplement with 0.1% Tween 20) at room temperature for 1 hr, and then incubated with primary antibodies, such as anti- STOM (a166623b, Abcam), anti-perilipin (9349, Cell Signaling), anti- PPARγ (2435, Cell Signaling), anti-C/EBPα (8178, Cell Signaling), anti-human STOM (M-14, Santa Cruz Biotechnology), anti-βTubulin (T2200, Sigma Aldrich), and anti-αActin antibodies, at 4 °C overnight. After washing three times with TBS-T, the PVDF membranes were incubated with horseradish peroxidase-conjugated secondary antibodies for 1 hr at room temperature, then treated with substrates (SuperSignal West Femto Maximum Sensitivity Substrate, Thermo Fisher Scientific), then visualized by ImageQuant (GE Healthcare Life Science).

Immunofluorescence

Cells seeded on coverslips were fixed with 3.7% paraformaldehyde (Sigma-Aldrich) at room temperature for 15 min, rinsed twice with PBS for 5 min, permeabilized and blocked using extraction buffer composed of 0.1 % saponin (Sigma-Aldrich) and 1 % BSA in PBS, for 1hr. Cells were then incubated with primary antibodies, including anti-STOM (a166623b, Abcam) and anti-perilipin (GT2781,GeneTex), at 4 ℃ overnight. After washing three times with wash buffer (PBS with 0.1 % saponin), cells were incubated with fluorochrome-conjugated secondary antibodies for 1 hr, and observed under a confocal microscope (LSM700, Zeiss).

FRAP assay

Adipocyte-like 3T3-L1 cells were incubated with 6μM of BODIPY™-FL-C_{12} (D3822, Invitrogen™) at 37°C overnight. After refreshing with complete medium, live cells were viewed under a confocal microscope (Zeiss, LSM700) using a 100x oil immersion objective. Selected regions were first bleached with 15 pulses of 100% laser power (combined 488 with 405 diode lasers), followed by time-lapse recording at 30-sec interval using normal imaging laser power.

Fatty acid uptake assay

For *in vitro* analysis, adipocyte-like 3T3-L1 cells were serum-starved in serum-free DMEM containing 1% sodium pyruvate for 1 hr at 37°C/5% CO2, changed to serum-free DMEM containing 1% sodium pyruvate and 10 μg/ml insulin for 30 min, then to 1X HBSS containing 20mM HEPES. Subsequently, 0.2 μM BODIPY-FL-C_{16} (Thermo) was added. The fluorescence (excitation: 485 nm and emission: 515 nm) was detected by ELISA reader (TECAN) using bottom-read mode and kinetic reading at a 30-sec interval. For *in vivo* analysis, 400 nM BODIPY™-FL-C_{16} was emulsified in 65 mg/ml BSA solution to prepare the probe solution. An amount of 1.2~1.5 ml (6~8% of body weight) probe solution was injected into the animal via tail vein. The mice were sacrificed and subcutaneous adipose tissues were resected for quantifications of fluorescence. Fat pads were homogenized using homogenizer (Roche MagNA Lyser Benchtop Homogenizer) for 45-sec at 3,000 r.p.m., and incubated at 65 °C for 30 min. After centrifugation at 12,000rpm for 10 min, fat layer was collected and subjected to fluorescence signal quantifications.

STOM transgenic mice and phenotype analyses

Transgenic mice overexpressing human *STOM* were generated by pronuclear microinjection. *STOM* was cloned into vector STOM-p1033, and RNA polymerase II large subunit promoter was used to drive expression in C57BL/6 mice as described previously [5]. The integration of the transgene was confirmed by PCR analysis of mouse tail DNA. Three to four weeks male *STOM* Tg and wild type littermates were fed with either chow diet or high-fat diet (D12492, 60 kcal% fat, Research Diets) for up to 20 weeks under free-feeding conditions. All of the mice were housed on a 12-hr light/dark cycle at 22°C. The blood biochemistry of *STOM* Tg and WT mice were

examined: fasting blood glucose and plasma insulin was determined by human blood glucose meter (Accu-chek Performa, Roche) and Mouse Ultrasensitive Insulin ELISA (80-INSMSU-E01, ALPCO), respectively. GOT and GPT were measured using Automated Clinical Chemistry Analyzer (FUJI DRI-CHEM 4000i).

Glucose tolerance tests

Mice fasted overnight were injected intraperitoneally with glucose solution (1 g/kg body weight). Blood glucose levels were measured at 0, 15, 30, 60, and 120 min after injection using a glucometer.

Histological analyses

The liver and adipose tissues were formalin-fixed and paraffin-embedded. Sections of WAT and the liver were stained with hematoxylin and eosin (H&E stain). All tissue images were obtained using the Aperio CS2 Digital Pathology Scanner (Leica) and analyzed via Imagescope software. The size of adipose cells was analyzed using the Fiji Adiposoft software to obtain the area of each and individual adipocyte.

Transcriptome expression analyses

Total RNA were extracted from cells using TRIzol® reagent and subjected to global transcriptome analysis using Mouse Genome Arrays (MTA-1_0, Affymetrix). The Transcriptome Analysis Console (TAC4.0) was used to process and analyze CEL files. We initially filtered for 11,264 probe sets annotated as locus type “coding”. Subsequently, 1,478 annotated coding genes were identified via exclusively a stringent threshold of p-value< 0.05 and FDR p-value< 0.001. Additionally, we further filtered for 379 genes via exclusively a stringent fold change threshold ≥ 3, or $\leq$ -3. The results were confirmed using qRT-PCR. The cDNAs were generated using SuperScript III First-Strand Synthesis System following the manufacturer’s protocol. To determine the expression of specific genes, quantitative real-time PCR (qRT-PCR) was performed using diluted cDNA in a total volume of 5ul with SYBR Green (Qiagen). Gene expression was normalized to the internal reference gene *Nono*, followed by calculation using $\Delta\,\Delta$CT method.

References

1. Gallagher PG, Forget BG. Structure, organization, and expression of the human band 7.2b gene, a candidate gene for hereditary hydrocytosis. *The Journal of biological chemistry* **270**, 26358-26363 (1995).

2. Fricke B, *et al.* The "stomatin" gene and protein in overhydrated hereditary stomatocytosis. *Blood* **102**, 2268-2277 (2003).

3. Zhu Y, *et al.* Stomatocytosis is absent in "stomatin"-deficient murine red blood cells. *Blood* **93**, 2404-2410 (1999).

4. Chen TW, Liu HW, Liou YJ, Lee JH, Lin CH. Over-expression of stomatin causes syncytium formation in nonfusogenic JEG-3 choriocarcinoma placental cells. *Cell biology international* **40**, 926-933 (2016).

5. Lee JH, *et al.* Lipid raft-associated stomatin enhances cell fusion. *FASEB journal : official publication of the Federation of American Societies for Experimental Biology* **31**, 47-59 (2017).

6. Snyers L, Umlauf E, Prohaska R. Association of stomatin with lipid-protein complexes in the plasma membrane and the endocytic compartment. *European journal of cell biology* **78**, 802-812 (1999).

7. Umlauf E, Csaszar E, Moertelmaier M, Schuetz GJ, Parton RG, Prohaska R. Association of stomatin with lipid bodies. *The Journal of biological chemistry* **279**, 23699-23709 (2004).

8. Mairhofer M, Steiner M, Mosgoeller W, Prohaska R, Salzer U. Stomatin is a major lipid-raft component of platelet alpha granules. *Blood* **100**, 897-904 (2002).

9. Genetet S, Desrames A, Chouali Y, Ripoche P, Lopez C, Mouro-Chanteloup I. Stomatin modulates the activity of the Anion Exchanger 1 (AE1, SLC4A1). *Scientific reports* **7**, 46170 (2017).

10. Montel-Hagen A, *et al.* Erythrocyte Glut1 triggers dehydroascorbic acid uptake in mammals unable to synthesize vitamin C. *Cell* **132**, 1039-1048 (2008).

11. Rungaldier S, Oberwagner W, Salzer U, Csaszar E, Prohaska R. Stomatin interacts with GLUT1/SLC2A1, band 3/SLC4A1, and aquaporin-1 in human erythrocyte membrane domains. *Biochimica et biophysica acta* **1828**, 956-966 (2013).

12. Brand J, *et al.* A stomatin dimer modulates the activity of acid-sensing ion channels. *The EMBO journal* **31**, 3635-3646 (2012).

13. Klipp RC, Cullinan MM, Bankston JR. Insights into the molecular mechanisms underlying the inhibition of acid-sensing ion channel 3 gating by stomatin. *J Gen Physiol* **152**, (2020).

14. Moshourab RA, Wetzel C, Martinez-Salgado C, Lewin GR. Stomatin-domain protein interactions with acid-sensing ion channels modulate nociceptor mechanosensitivity. *The Journal of physiology* **591**, 5555-5574 (2013).

15. Schwartz MW, *et al.* Obesity Pathogenesis: An Endocrine Society Scientific Statement. *Endocr Rev* **38**, 267-296 (2017).

16. Sandholt CH, Hansen T, Pedersen O. Beyond the fourth wave of genome-wide obesity association studies. *Nutr Diabetes* **2**, e37 (2012).

17. James WPT. Obesity: A Global Public Health Challenge. *Clin Chem* **64**, 24-29 (2018).

18. Swinburn BA, *et al.* The global obesity pandemic: shaped by global drivers and local environments. *Lancet* **378**, 804-814 (2011).

19. Wabitsch M, *et al.* Severe Early-Onset Obesity Due to Bioinactive Leptin Caused by a p.N103K Mutation in the Leptin Gene. *J Clin Endocrinol Metab* **100**, 3227-3230 (2015).

20. Haslam DW, James WP. Obesity. *Lancet* **366**, 1197-1209 (2005).

21. Albuquerque D, Stice E, Rodriguez-Lopez R, Manco L, Nobrega C. Current review of genetics of human obesity: from molecular mechanisms to an evolutionary perspective. *Mol Genet Genomics* **290**, 1191-1221 (2015).

22. Xia Q, Grant SF. The genetics of human obesity. *Ann N Y Acad Sci* **1281**, 178-190 (2013).

23. McLaughlin T*, et al.* Adipose Cell Size and Regional Fat Deposition as Predictors of Metabolic Response to Overfeeding in Insulin-Resistant and Insulin-Sensitive Humans. *Diabetes* **65**, 1245-1254 (2016).

24. Haczeyni F, Bell-Anderson KS, Farrell GC. Causes and mechanisms of adipocyte enlargement and adipose expansion. *Obes Rev* **19**, 406-420 (2018).

25. Pilch PF*, et al.* Cellular spelunking: exploring adipocyte caveolae. *J Lipid Res* **48**, 2103-2111 (2007).

26. Kuerschner L, Moessinger C, Thiele C. Imaging of lipid biosynthesis: how a neutral lipid enters lipid droplets. *Traffic* **9**, 338-352 (2008).

27. Yang H, Galea A, Sytnyk V, Crossley M. Controlling the size of lipid droplets: lipid and protein factors. *Curr Opin Cell Biol* **24**, 509-516 (2012).

28. Ehehalt R, Fullekrug J, Pohl J, Ring A, Herrmann T, Stremmel W. Translocation of long chain fatty acids across the plasma membrane--lipid rafts and fatty acid transport proteins. *Mol Cell Biochem* **284**, 135-140 (2006).

29. Harder T, Scheiffele P, Verkade P, Simons K. Lipid domain structure of the plasma membrane revealed by patching of membrane components. *The Journal of cell biology* **141**, 929-942 (1998).

30. Bostrom P*, et al.* SNARE proteins mediate fusion between cytosolic lipid droplets and are implicated in insulin sensitivity. *Nat Cell Biol* **9**, 1286-1293 (2007).

31. Tansey JT, *et al.* Perilipin ablation results in a lean mouse with aberrant adipocyte lipolysis, enhanced leptin production, and resistance to diet-induced obesity. *Proceedings of the National Academy of Sciences of the United States of America* **98**, 6494-6499 (2001).

32. Miyoshi H, *et al.* Control of adipose triglyceride lipase action by serine 517 of perilipin A globally regulates protein kinase A-stimulated lipolysis in adipocytes. *The Journal of biological chemistry* **282**, 996-1002 (2007).

33. Keller P, *et al.* Fat-specific protein 27 regulates storage of triacylglycerol. *The Journal of biological chemistry* **283**, 14355-14365 (2008).

34. Liu K, *et al.* Functional analysis of FSP27 protein regions for lipid droplet localization, caspase-dependent apoptosis, and dimerization with CIDEA. *Am J Physiol Endocrinol Metab* **297**, E1395-1413 (2009).

35. Sun Z, *et al.* Perilipin1 promotes unilocular lipid droplet formation through the activation of Fsp27 in adipocytes. *Nature communications* **4**, 1594 (2013).

36. Yuan SM, *et al.* Over-expression of PPAR-gamma2 gene enhances the adipogenic differentiation of hemangioma-derived mesenchymal stem cells in vitro and in vivo. *Oncotarget* **8**, 115817-115828 (2017).

37. Farmer SR. Transcriptional control of adipocyte formation. *Cell Metab* **4**, 263-273 (2006).

38. Bost F, Aouadi M, Caron L, Binetruy B. The role of MAPKs in adipocyte differentiation and obesity. *Biochimie* **87**, 51-56 (2005).

39. Aubert J, Belmonte N, Dani C. Role of pathways for signal transducers and activators of transcription, and mitogen-activated protein kinase in adipocyte differentiation. *Cell Mol Life Sci* **56**, 538-542 (1999).

40. Ghaben AL, Scherer PE. Adipogenesis and metabolic health. *Nat Rev Mol Cell Biol* **20**, 242-258 (2019).

41. Green H, Meuth M. An established pre-adipose cell line and its differentiation in culture. *Cell* **3**, 127-133 (1974).

42. Dutta-Roy AK. Cellular uptake of long-chain fatty acids: role of membrane-associated fatty-acid-binding/transport proteins. *Cell Mol Life Sci* **57**, 1360-1372 (2000).

43. Wetzel C, *et al.* Small-molecule inhibition of STOML3 oligomerization reverses pathological mechanical hypersensitivity. *Nat Neurosci* **20**, 209-218 (2017).

44. Prusty D, Park BH, Davis KE, Farmer SR. Activation of MEK/ERK signaling promotes adipogenesis by enhancing peroxisome proliferator-activated receptor gamma (PPARgamma) and C/EBPalpha gene expression during the differentiation of 3T3-L1 preadipocytes. *The Journal of biological chemistry* **277**, 46226-46232 (2002).

45. Scioli MG, Bielli A, Gentile P, Mazzaglia D, Cervelli V, Orlandi A. The biomolecular basis of adipogenic differentiation of adipose-derived stem cells. *Int J Mol Sci* **15**, 6517-6526 (2014).

46. Wee P, Wang Z. Epidermal Growth Factor Receptor Cell Proliferation Signaling Pathways. *Cancers (Basel)* **9**, (2017).

47. Sigismund S, Argenzio E, Tosoni D, Cavallaro E, Polo S, Di Fiore PP. Clathrin-mediated internalization is essential for sustained EGFR signaling but dispensable for degradation. *Developmental cell* **15**, 209-219 (2008).

48. Lajoie P, Kojic LD, Nim S, Li L, Dennis JW, Nabi IR. Caveolin-1 regulation of dynamin-dependent, raft-mediated endocytosis of cholera toxin-B sub-unit occurs independently of caveolae. *Journal of cellular and molecular medicine* **13**, 3218-3225 (2009).

49. Lajoie P, Goetz JG, Dennis JW, Nabi IR. Lattices, rafts, and scaffolds: domain regulation of receptor signaling at the plasma membrane. *The Journal of cell biology* **185**, 381-385 (2009).

50. Disanza A, Frittoli E, Palamidessi A, Scita G. Endocytosis and spatial restriction of cell signaling. *Mol Oncol* **3**, 280-296 (2009).

51. Wilfling F, Haas JT, Walther TC, Farese RV, Jr. Lipid droplet biogenesis. *Curr Opin Cell Biol* **29**, 39-45 (2014).

52. Gross DA, Zhan C, Silver DL. Direct binding of triglyceride to fat storage-inducing transmembrane proteins 1 and 2 is important for lipid droplet formation. *Proceedings of the National Academy of Sciences of the United States of America* **108**, 19581-19586 (2011).

53. Wilfling F*, et al.* Triacylglycerol synthesis enzymes mediate lipid droplet growth by relocalizing from the ER to lipid droplets. *Developmental cell* **24**, 384-399 (2013).

54. Walther TC, Farese RV, Jr. Lipid droplets and cellular lipid metabolism. *Annu Rev Biochem* **81**, 687-714 (2012).

55. Yu J, Li P. The size matters: regulation of lipid storage by lipid droplet dynamics. *Sci China Life Sci* **60**, 46-56 (2017).

56. Gao G*, et al.* Control of lipid droplet fusion and growth by CIDE family proteins. *Biochim Biophys Acta Mol Cell Biol Lipids* **1862**, 1197-1204 (2017).

57. Simard JR, Pillai BK, Hamilton JA. Fatty acid flip-flop in a model membrane is faster than desorption into the aqueous phase. *Biochemistry* **47**, 9081-9089 (2008).

58. Pohl J, Ring A, Korkmaz U, Ehehalt R, Stremmel W. FAT/CD36-mediated long-chain fatty acid uptake in adipocytes requires plasma membrane rafts. *Mol Biol Cell* **16**, 24-31 (2005).

59. Lapatsina L*, et al.* Regulation of ASIC channels by a stomatin/STOML3 complex located in a mobile vesicle pool in sensory neurons. *Open biology* **2**, 120096 (2012).

60. Price MP, Thompson RJ, Eshcol JO, Wemmie JA, Benson CJ. Stomatin modulates gating of acid-sensing ion channels. *The Journal of biological chemistry* **279**, 53886-53891 (2004).

61. Muir LA, *et al.* Adipose tissue fibrosis, hypertrophy, and hyperplasia: Correlations with diabetes in human obesity. *Obesity (Silver Spring)* **24**, 597-605 (2016).

Acknowledgements

The authors acknowledge Mouse Genome Arrays analysis provided by Genomics Center for Clinical and Biotechnological Applications of Cancer Progression Research Center, National Yang-Ming University. Genomics Center for Clinical and Biotechnological Applications is supported by National Core Facility for Biopharmaceuticals (NCFB), Ministry of Science and Technology. We thank the Taiwan Mouse Clinic (TMC) from the Academia Sinica and Taiwan Animal Consortium for technical support in metabolism related experiments. We are deeply grateful to Dr. Kate Hua (NYMU), Chian-Feng Chen (NYMU), Tzuu-Shuh Jou (NTU), Jia-Fwu Shyu (NDMC) and Hong-Yu Chien (TCH) for their helpful scientific suggestions; Dr. Li-Li Li (LTRI, Canada) for her helpful proof-reading of the manuscript. This work was supported by the Ministry of Education, Aim for the Top University Plan: MOST 109-2740-B-010-002. The authors declare no conflicts of interest. NYMU: National Yang-Ming University. NTU: National Taiwan University. NDMC: National Defense Medical Center. TCH: Taipei City Hospital.

Author contributions

S.-C. Wu, W.-N. Lian, C.-Y. Tung and C.-H. Lin designed the research; S.-C. Wu and Y.-M. Lio performed the research and analyzed the data; S.-C. Wu, J.-H. Lee, H.-W. Liu and T.-W. Chen contributed microscopic approaches; W.-J. Lin, C.-Y. Chen and C.-Y. Yang contributed materials; and S.-C. Wu, and C.- H. Lin wrote the manuscript.

Competing financial interests

The authors declare that no competing financial interests exist.

Supplemental

Video 1

The time-lapse recording under phase contrast and fluorescence microscopy of the sequence of a LD-LD fusion event within a live adipocyte-like 3T3-L1 cell transfected with hSTOM-RFP. Time is shown in hr:min.

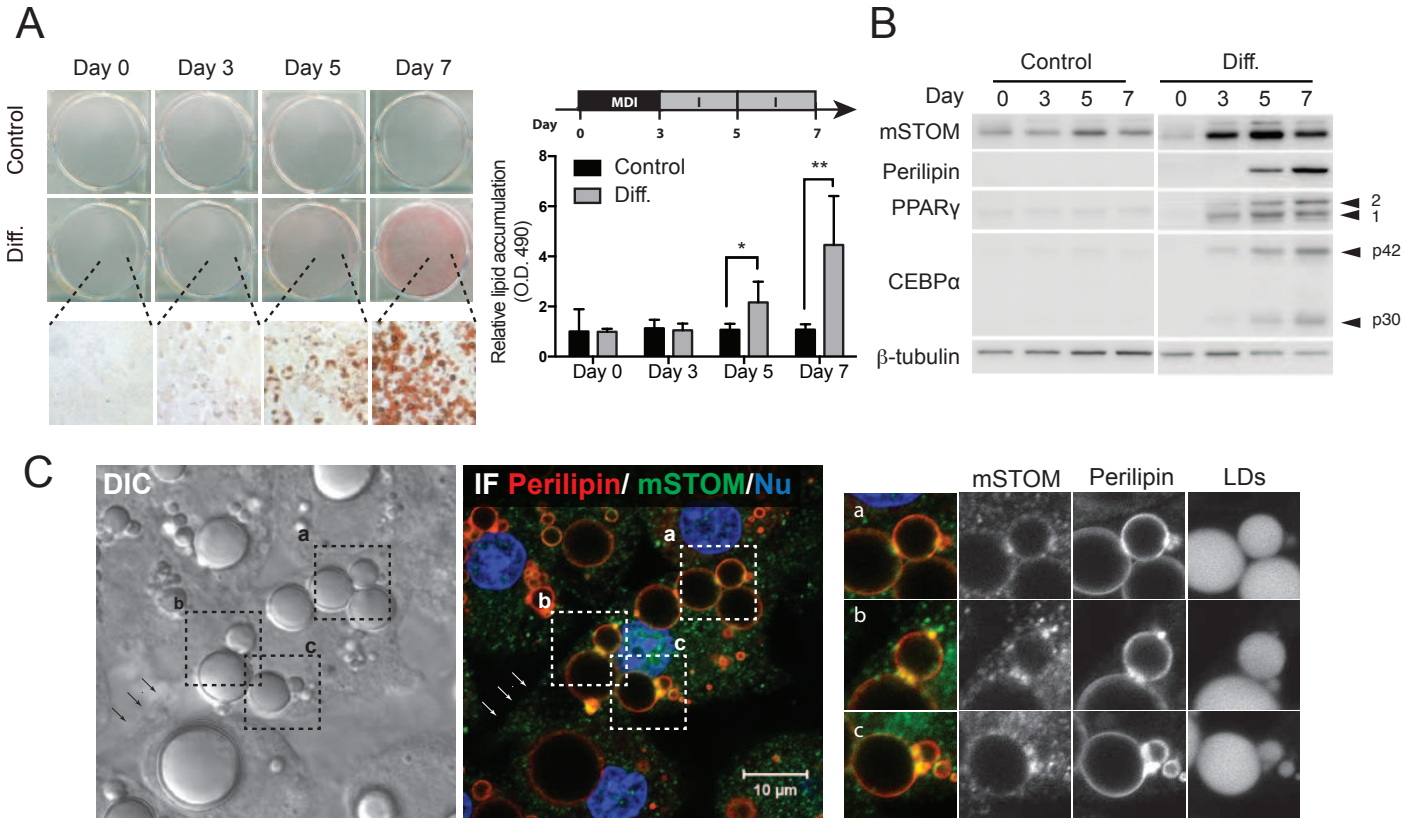

Figure 1: Stomatin expressions increased during adipogenesis. A) Mouse 3T3-L1 fibroblasts were treated with MDI induction medium (Diff.) or control vehicle. On day 0, 3, 5, 7 after induction, cells were stained with Oil Red O and observed under microscopy. The amounts of lipid accumulation for individual culture plates were quantified by measuring absorbance at 490 nm (OD 490). Mean ± s.d. for six independent experiments. **P<0.01 and ****P<0.0001 by two-way ANOVA analysis. **B)** On the day after induction as indicated, Western blotting analyses revealed increased expressions of mouse stomatin (mSTOM), perilipin, PPARγ and C/EBPα. **C)** Subcellular distributions of endogenous stomatin (green) and perilipin (red) on cells after 7-day induction were observed by DIC and immunofluorescence microscopy (IF). Cell nuclei were revealed by DNA stain (blue). Perilipin and mSTOM were found colocalized on vesicular membranes of lipid droplets (LDs) (inset). Bar = 10 μm.

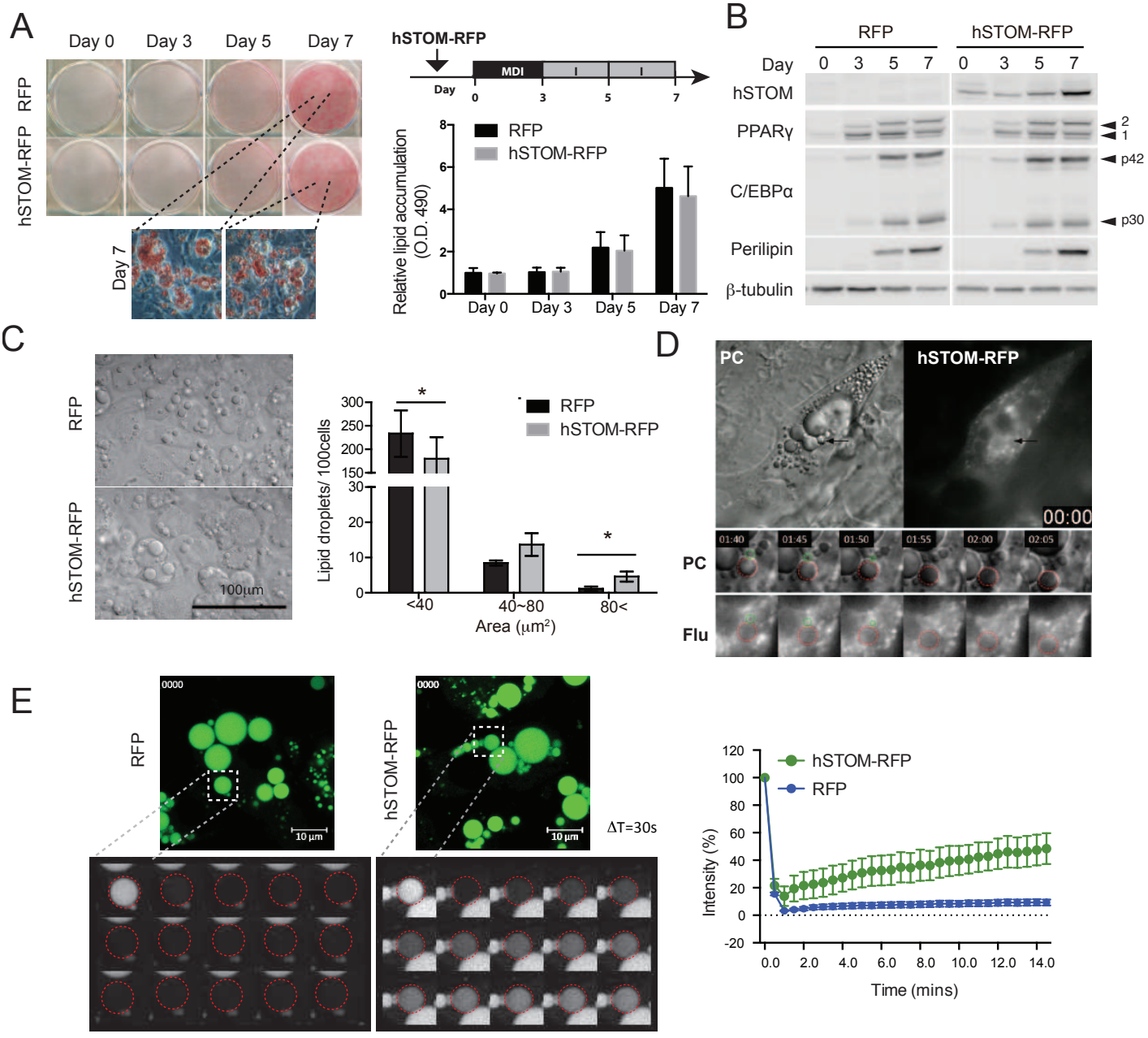

Figure 2: Overexpression of stomatin promoted lipid droplet growth and facilitated fatty acid uptake in adipocyte-like cells. A) Mouse 3T3-L1 cells over-expressing exogenous human stomatin conjugated with RFP (hSTOM-RFP) or RFP as control, were induced to differentiate into adipocyte-like cells. Lipid contents of the cells were visualized by Oil Red O staining and OD measured at 490nm. Mean ± s.d. for four independent experiments. **B)** Exogenous human stomatin (hSTOM), PPARγ, C/EBPα, and perilipin were examined by Western blotting. **C)** The numbers and sizes of lipid droplets (LDs) in adipocyte-like cells (on day 7 of induction) were quantified after AdipoRed staining and plotted as a function of LD areas. There were larger LDs (> 80 μm2) found in cells over-expressing stomatin than the control cells, which contained mostly small (< 40 μm2) LDs. Mean ± s.e.m. for three independent experiments. *P<0.05 by paired t-test. Bar = 100 μm. **D)** The time-lapse recording of a LD-LD fusion event (arrow) within a live adipocyte-like 3T3-L1 cell transfected with hSTOM-RFP. A small LD (green dashed circle) was noted to fuse with a large LD (red dashed circle) then disappeared. Time of image tiles is shown as hr : min. PC: phase-contrast microscopy; Flu: fluorescence microscopy. **E)** Fluorescence recovery after photobleaching (FRAP) experiments were done on cells expressing hSTOM-RFP (n = 7) or RFP (n = 10). Adipocyte-like cells were pre-treated with BODIPY-FL-C12 fatty acid. Photobleaching was done at a randomly selected LD (dashed box); Afterbleaching, fluorescence recovery, as % of original intensity, was recorded by time-lapse microscopy at a 30-sec interval. Mean ± s.e.m. for three independent experiments. Bar = 10 μm. **F)** Adipocyte-like cells expressing FLAG-conjugated human stomatin (hSF) or vector control (V) were treated with 0.2 μM fluorescently-labeled fatty acid (BODIPY-FL-C16) to measure uptake of extracellular fatty acid into the cells, or with fluorescent tag (BODIPY-FL) as a control to measure non-specific leak of BODIPY-FL into the cell. Intracellular accumulations of fluorescence over time were recorded and plotted as a function of time. Mean ± s.e.m. for three independent experiments.

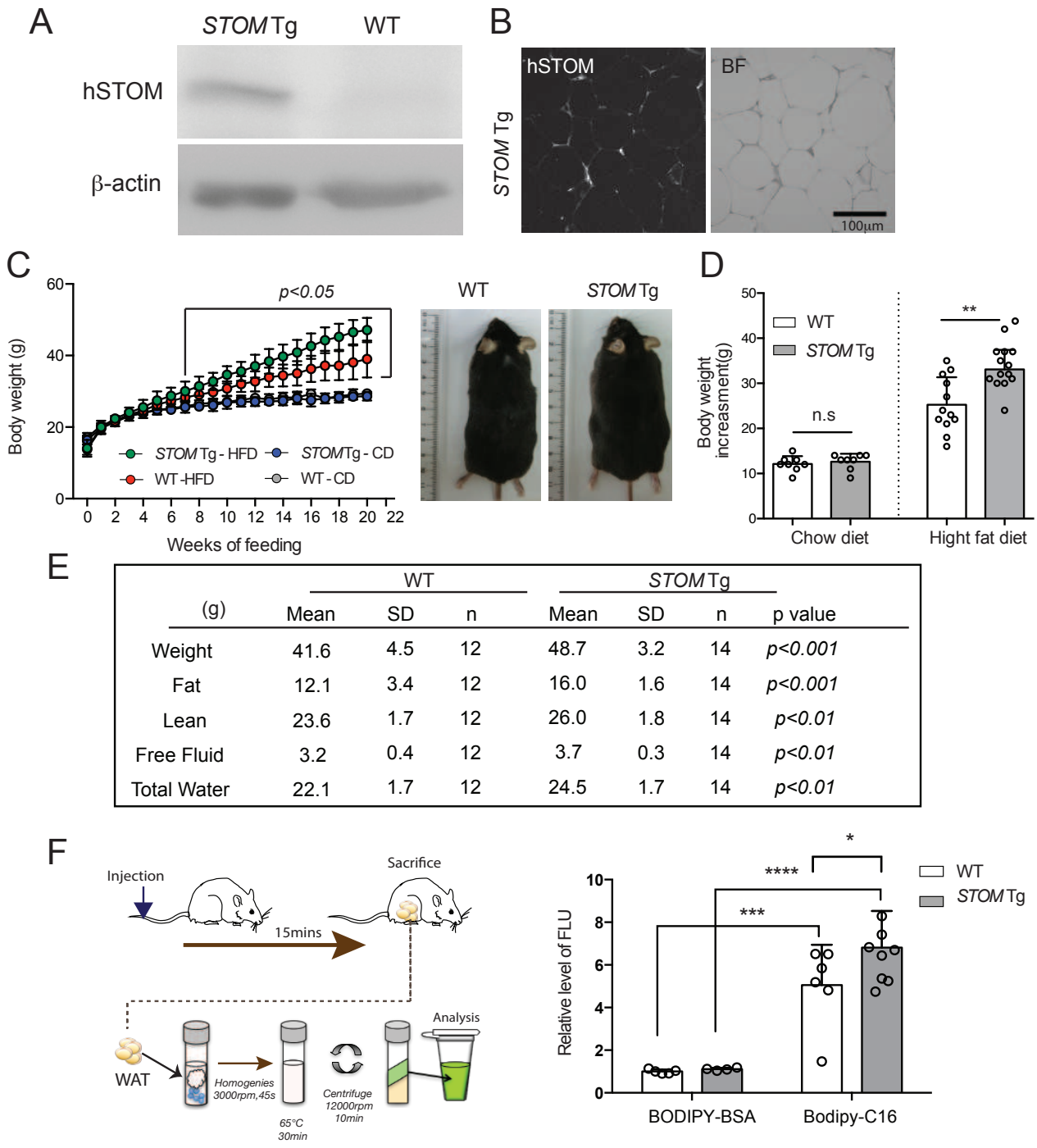

(g)	WT Mean	WT SD	WT n	STOM Tg Mean	STOM Tg SD	STOM Tg n	p value
Weight	41.6	4.5	12	48.7	3.2	14	*p<0.001*
Fat	12.1	3.4	12	16.0	1.6	14	*p<0.001*
Lean	23.6	1.7	12	26.0	1.8	14	*p<0.01*
Free Fluid	3.2	0.4	12	3.7	0.3	14	*p<0.01*
Total Water	22.1	1.7	12	24.5	1.7	14	*p<0.01*

Figure 3: Stomatin transgenic mice fed with high-fat diet were more obese than the control mice. A) Western blotting revealed high expression of human stomatin (hSTOM) in stomatin transgenic mice (STOM Tg). **B)** The exogenous hSTOM proteins were present mainly on surface of the adipocyte plasma membrane in fat tissues of STOM Tg mice. **C)** Body weight changes of STOM Tg and wild type (WT) mice fed with regular chow diet (CD) or high-fat diet (HFD) for 20 weeks. Representative photos of the mice are shown. **D)** Body weight increments after 20-week feeding were measured. Each dot represents one mouse. While no difference was noticed in animals fed with CD, body weight gains were significantly higher in HFD-fed STOM Tg, compared with HFD-fed WT mice. Mean ± s.d. is shown. n.s = non-significant. **P<0.01 by unpaired t-test. **E)** The mass of whole body, fat, lean, free fluid, and total water were calculated for HFD-fed STOM Tg and HFD-fed WT mice. **F)** Fatty acid uptake was measured in vivo. Fluorescently-labeled BODIPY-FL-C16 fatty acid, or BODIPY-BSA, were injected into tail vein of STOM Tg mice or WT mice. After 15 min, aqueous portions of white adipose tissue (WAT) from the animal were extracted and fluorescence signals that represented lipid uptake were quantified. Data shown are fold changes of fluorescence intensity using BODIPY-BSA injected to WT mice as the reference. Each dot represents one mouse. Mean ± s.d. for three independent experiments. *P<0.05, **P<0.01, and ****P<0.0001 by two-way ANOVA. BODIPY-FL-C16: 4,4-Difluoro-5,7-Dimethyl-4-Bora-3a,4a-Diaza-s-Indacene-3-Hexadecanoic Acid; BSA: bovine serum albumin

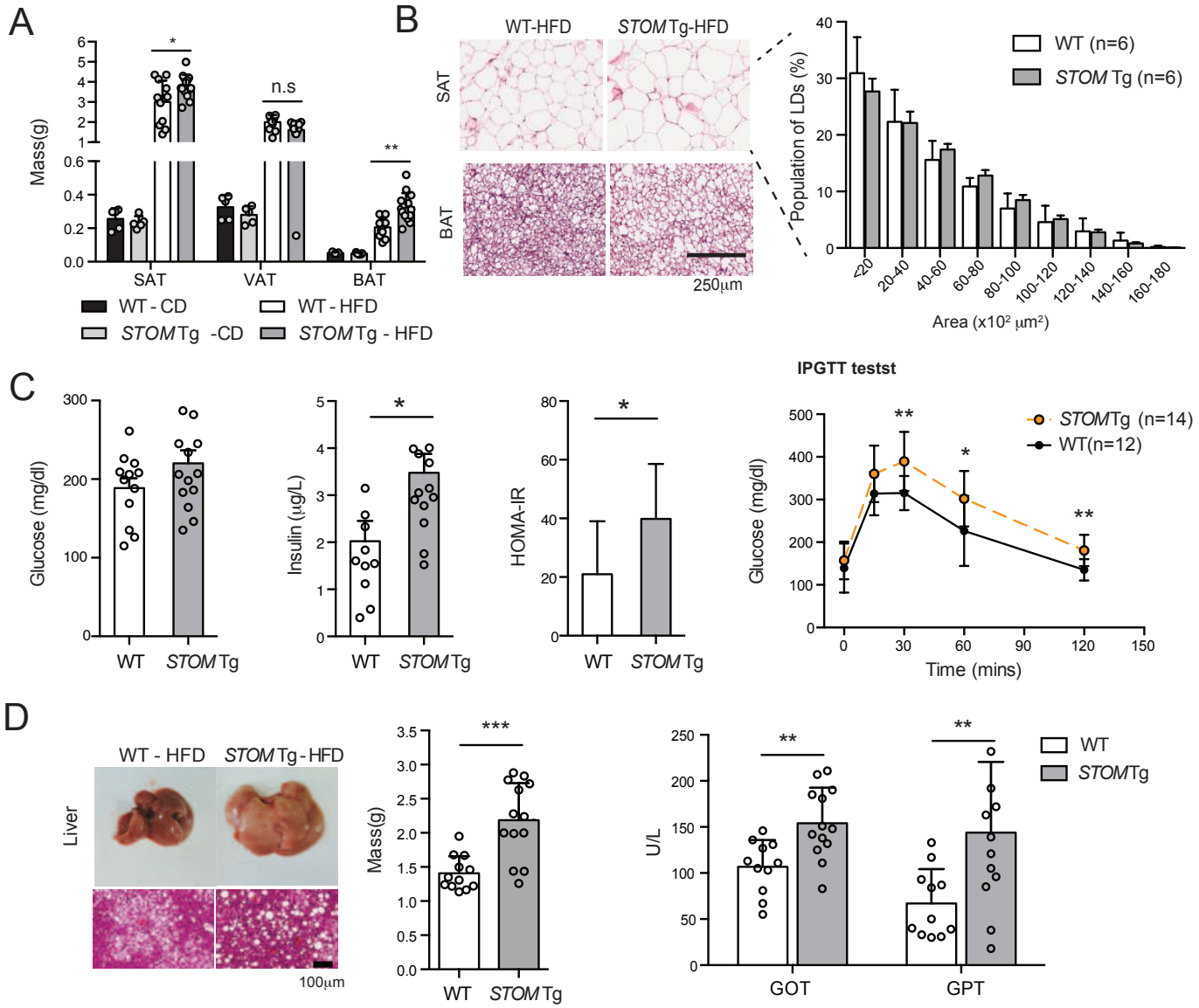

Figure 4: Stomatin transgenic mice fed with high-fat diet exhibited adipocyte hypertrophy and metabolism disorders. A) The weights of subcutaneous adipose tissue (SAT), visceral adipose tissue (VAT) and brown adipose tissue (BAT) in stomatin transgenic mice (STOM Tg) or wild type mice (WT) fed with regular chow diet (CD) or high-fat diet (HFD) for 20 weeks were measured. **B)** Representative H&E stained histopathological sections of SAT, and BAT from HFD-fed STOM Tg or HFD-fed WT mice. Histogram analyses of sizes of adipocytes are shown. Bar = 250μm. **C)** After HFD-feeding for 20 weeks, the animal's fasting glucose, serum insulin, homeostatic model assessment of insulin resistance (HOMA-IR), and intraperitoneal glucose tolerance test (IPGTT) were examined. **D)** The mass of liver of STOM Tg or WT mice, fed with HFD for 20 weeks, were weighed. Fatty liver changes revealed by histopathological sections and high level of serum glutamate oxaloacetate transaminase (GOT) and glutamate pyruvate transaminase (GPT) indicated impaired hepatic functions in STOM Tg mice, compared to WT mice. Bar = 100μm. Each dot represents one mouse. Mean ± s.d. is shown. n.s = non-significant. *P<0.05, **P<0.01, and ***P<0.001 by unpaired t-test.

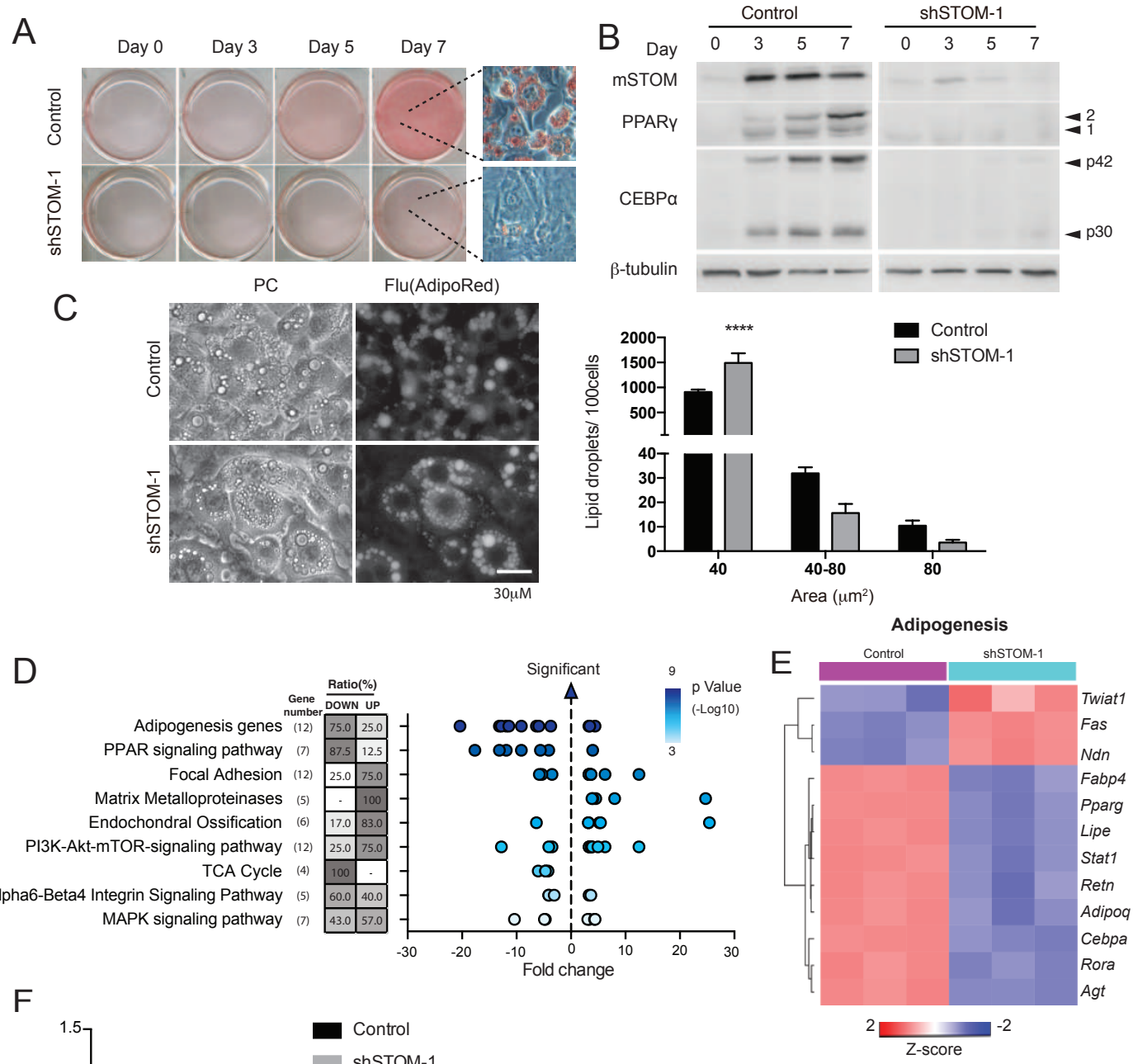

Figure 5: Decreased stomatin expression affected adipogenesis and inhibited lipid droplet growth. A) Stomatin knockdown was done by transduction of shRNA of Stomatin gene into 3T3-L1 cells generating shSTOM-1 cells or shSTOM-2 cells. After induction of adipogenic differentiation, shSTOM-1 and control cells were stained with Oil Red O. Cells after 7-day induction are shown using high-power microscopy. **B)** On the day after induction as indicated, Western blotting analyses revealed decreased expression of mouse stomatin (mSTOM) by knockdown. Adipogenic proteins, including PPARγ, and C/EBPα were also down-regulated. **C)** On day 7 of adipogenic differentiation, adipocyte-like shSTOM-1 cells were stained with AdipoRed and observed under phase-contrast (PC) and fluorescence (Flu) microscopy. The size of lipid droplets (LDs) were measured, and their number per 100 adipocytes were calculated. Histogram analyses showed more small LDs (< 40 μm^2) and fewer large (> 80 μm^2) LDs in shSTOM-1 cells than the control. Mean ± s.d. for three independent experiments. ****P<0.0001 by two-way ANOVA. Bar = 30 μm. **D)** Transcriptome analyses of adipocyte-like shSTOM-1 and control cells after induction for 7 days. From the data of microarray assays, scatter plots revealed enriched Wiki pathways in shSTOM-1 cells comparing to the control. For a given pathway, ratio of gene number being up- or down-regulated in that pathway were determined, and plotted as function of fold change. Each dot represents one gene. The color of the dots represents the range of P-values related to the indicated pathway. **E)** Heat map of adipogenesis gene obtained from the enrichment-based cluster analysis of the Wiki pathway. **F)** Real-time qPCR analyses to validate the changed genes revealed by microarray assays. Data shown are fold changes relative to Nono mRNA level. Mean ± s.d. for three independent experiments. ***P<0.001 by unpaired t-test.

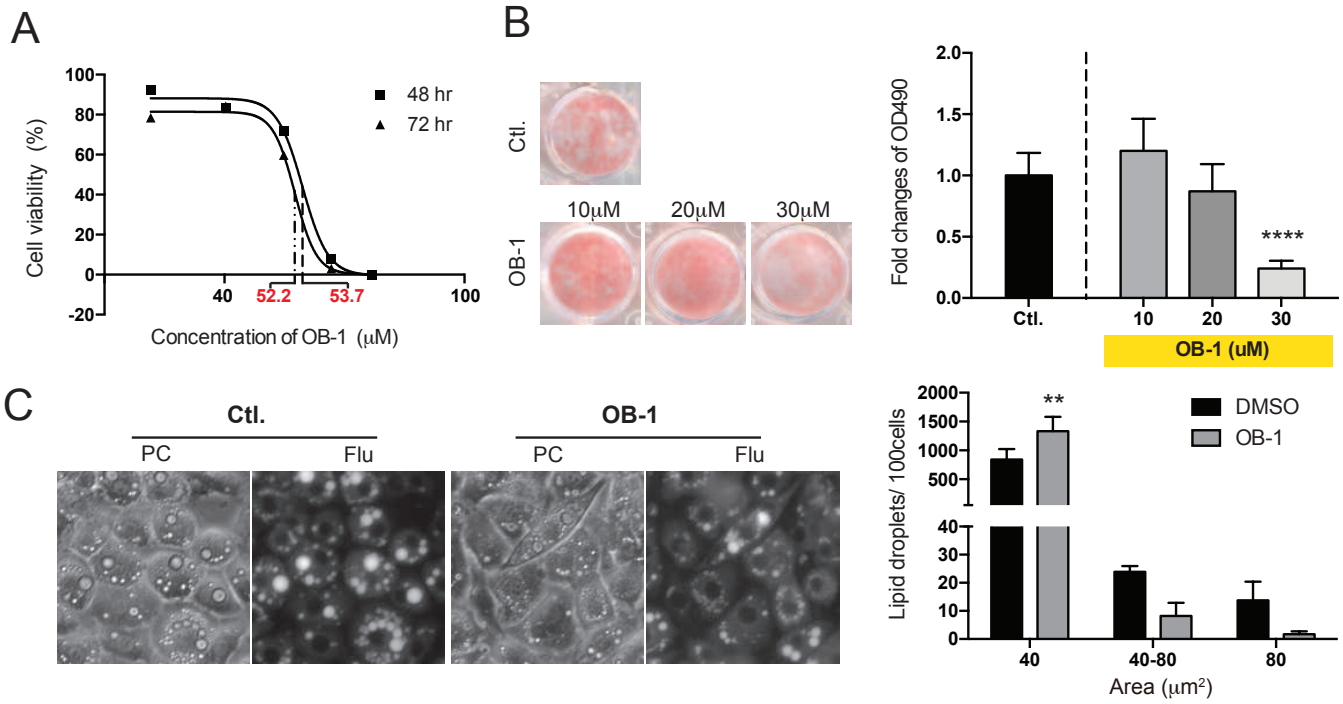

Figure 6: Stomatin inhibitor OB-1 inhibited adipogenesis and hindered lipid droplet growth. A) Cell viability after OB-1 treatments for 48h or 72h were tested by MTT assays. LC50 of OB-1 were calculated from three independent experiments. **B)** Culture adipocyte-like 3T3-L1 plates treated with or without OB-1 at concentrations indicated, were stained with Oil Red O and subjected to OD 490 quantifications. Note OB-1 inhibited adipogenesis in a dose-dependent manner, compared to the control DMSO treatment. Each OB-1 treatment data was normalized to the corresponding DMSO vehicle control; fold changes are shown. Mean ± s.d. for three independent experiments (n=9 for each experiment). ****P<0.0001 by one-way ANOVA. **C)** Adipocyte-like 3T3-L13T3-L1 cells after 7-day induction were treated with 25μM OB-1 or control vehicle, and stained with AdipoRed. The cells were observed under phase contrast (PC) or fluorescence microscopy (Flu) to determine the numbers and sizes of LD. Histogram analyses showed increased small LDs (< 40 μm^2) and decreased large (> 80 μm^2) LDs after OB-1 treatments, compared to the control. Mean ± s.d. for three independent experiments. **P<0.01 by two-way ANOVA. Bar = 30 μm.

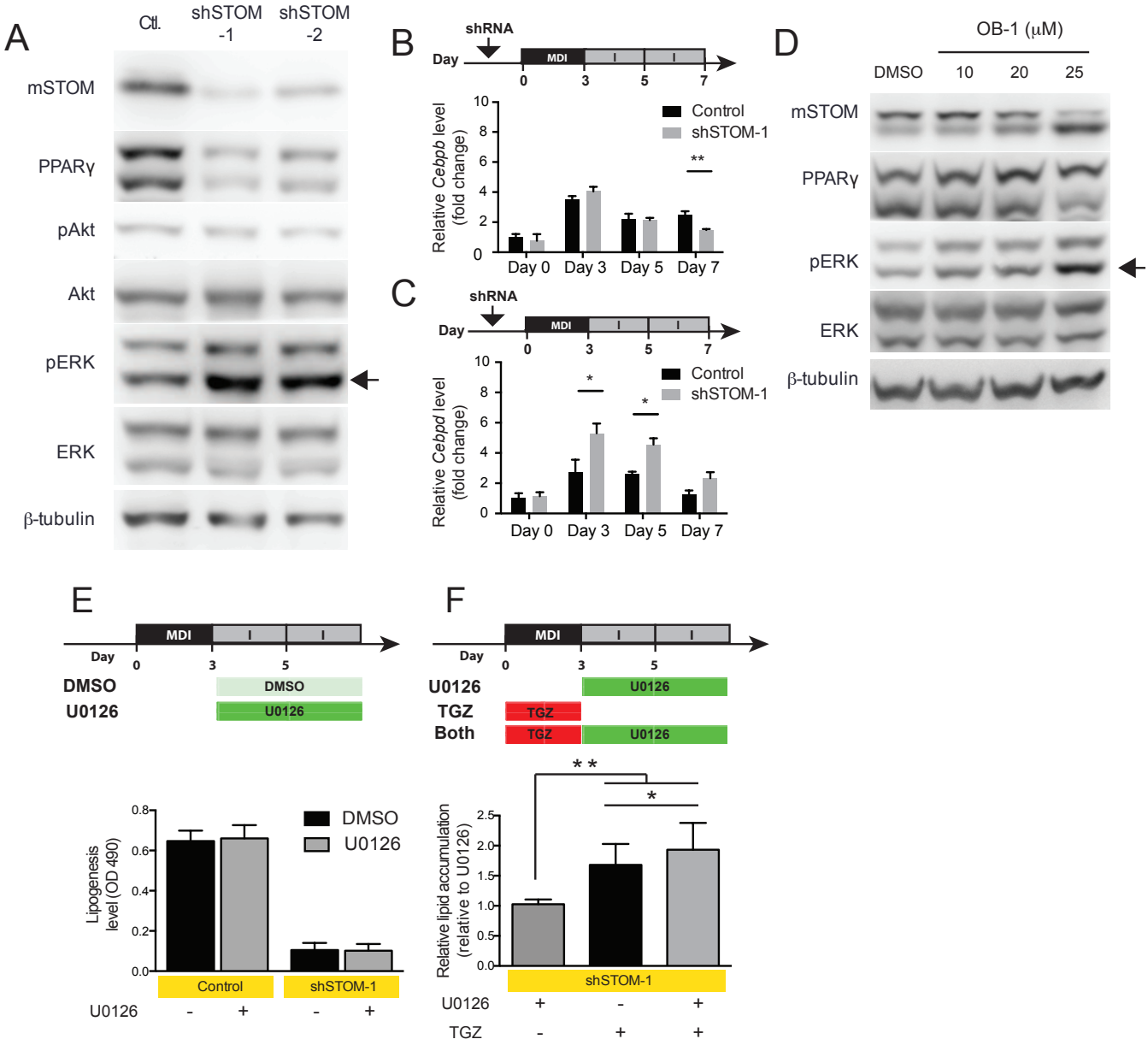

Figure 7: Knockdown of stomatin activated ERK-pathway. A) shRNA were transducted into 3T3-L1 cells to knockdown stomatin and generating shSTOM-1 and shSTOM-2 cells. After induction of differentiation, Western blotting analyses were done. Although Akt pathway remained unchanged, the ERK pathway was activated as evidenced by increased pERK (arrow). **B, C)** Expressions of early adipogenic genes, Cebpb and Cebpd, were examined at mRNA level by qPCR. **B)** Expressions of Cebpb increased in the first three days of adipogenic differentiation, and subsequently decreased. Knockdown of stomatin (exemplified by shSTOM-1 cells) did not significantly influence this pattern. **C)** Expressions of Cebpd gene also exhibited a transient early increase then declined; however, knockdown of stomatin appeared to significantly increase and maintain Cebpd expression at a relatively higher level than the control. The house-keeping Nono gene was used as the reference for qPCR exoeriments. *P<0.05 by unpaired t-test. **D)** Treating adipocyte-like cells with stomatin inhibitor OB-1 also resulted in activation of ERK pathway, evidenced by increased pERK (arrow). **E)** Levels of lipogenesis by adipocyte-like 3T3-L1 cells were quantified by measuring OD 490 after Oil Red O staining. Treating shSTOM-1 cells with 10μM U0126, an ERK pathway inhibitor, from day3 to day 7, did not reverse the lipogenesis inhibition caused by stomatin knockdown. **F)** On the other hand, treating shSTOM-1cells with TGZ, a PPARγ activator, in the first three days of adipogenic differentiation, was able to partially recover the knockdown-caused lipogenesis deficit; treating shSTOM-1cells with both TGZ and U0126 was noted to further increase lipid accumulation. Mean ± s.d. for six independent experiments. *P<0.05, and **P<0.01 by one-way ANOVA. qPCR: quantitative real-time PCR.

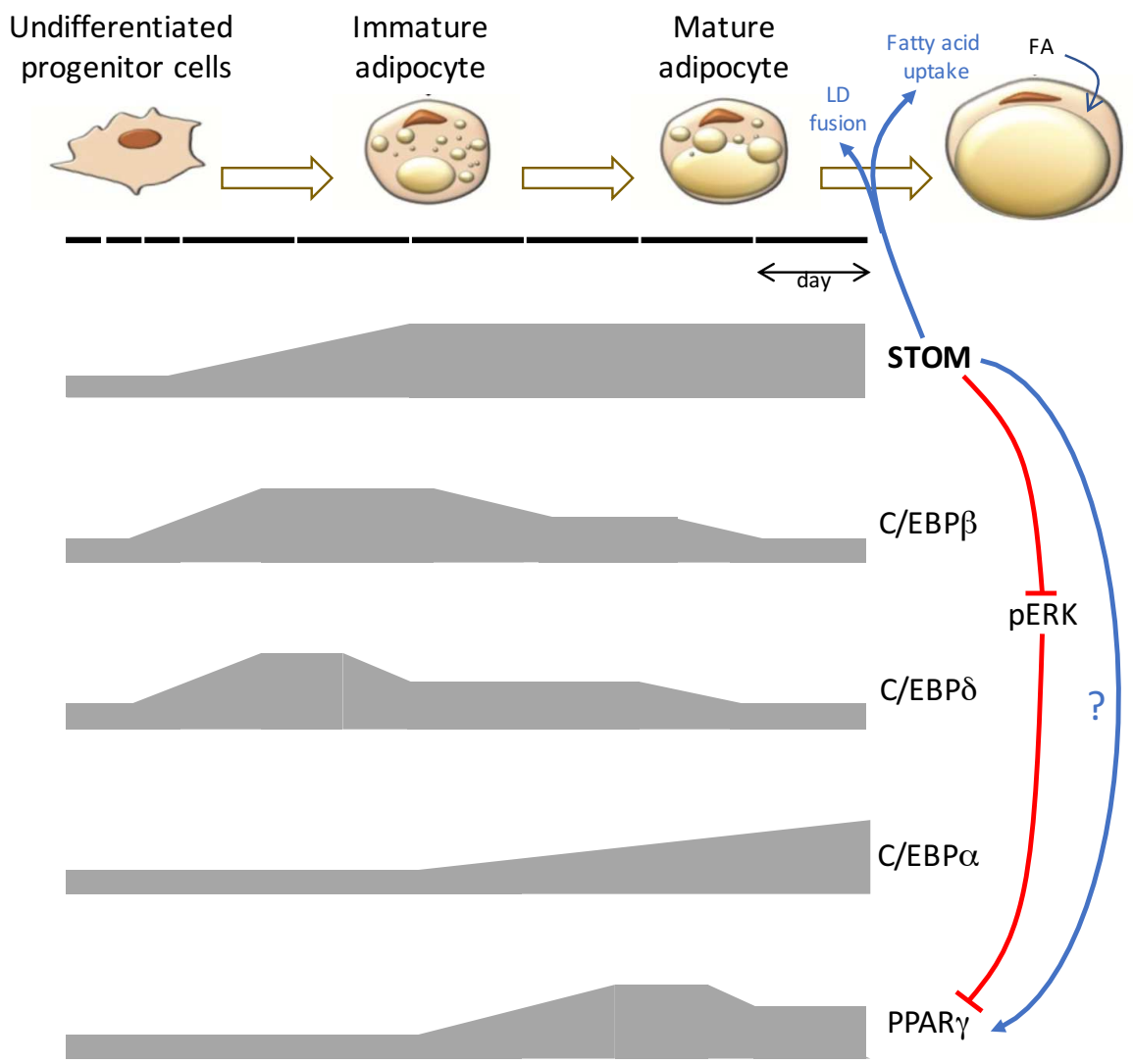

Figure 8: Stomatin's roles in modulating adipogenic differentiation and lipogenesis. Undifferentiated progenitor cells can be induced to undergo adipogenic differentiation to become immature adipocytes, and further develop into mature adipocytes, characterized by fatty acid uptake, production of lipid, and fusions and enlargements of lipid droplets (LDs). Dynamic expressions of adipogenic genes along this process are depicted. Stomatin progressively increases during adipocyte differentiation and maturation, and participates not only in fatty acid uptake and LD fusions, but also in modulation of adipogenic gene expressions. By inhibiting pERK, stomatin activates PPARγ: resulting in adipocyte maturation and lipogenesis. Stomatin also plays a role in regulating early phase adipogenic genes, such as C/EBPβ and C/EBPδ through currently unknown mechanisms. C/EBP: CCAAT/enhancer binding protein; PPARγ: peroxisome proliferator-activated receptor-γ.

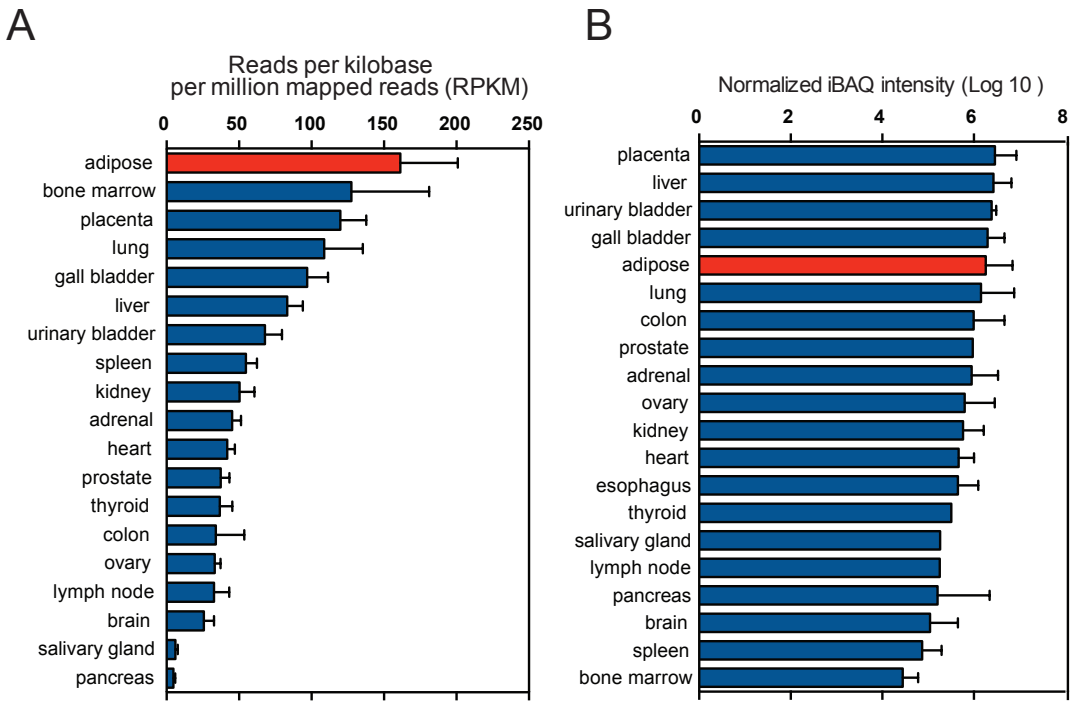

Supplemental Figure 1: In silico analyses of stomatin mRNA and proteins in different human tissues. A) The bar charts were reproduced based on the data of NCBI: https://www.ncbi.nlm.nih.gov/gene/2040?report=expression&bioproject=PRJEB4337, containing RNA sequencing of total RNA from 20 human tissues. Adipose tissues expressed the highest amount of mRNA among all tissues examined. Mean ± s.d. is shown. **B)** The bar charts were reproduced using ProteomicsDB: https://www.proteomicsdb.org/proteomicsdb/#protein/proteinDetails/54374/expression. The error bars indicate the lowest and highest abundance level for the selected protein.

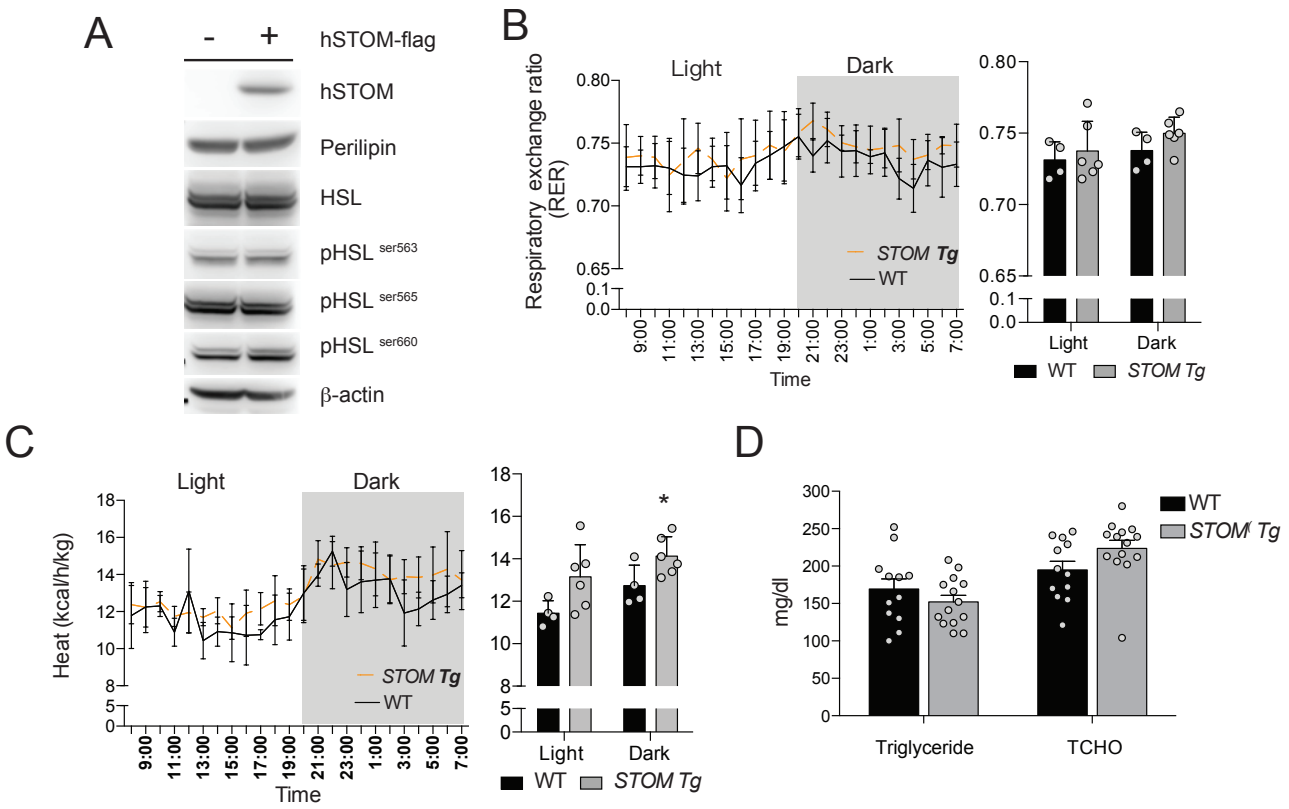

Supplemental Figure 2: Regulations of lipid metabolisms by stomatin. A) Hormone-sensitive lipase (HSL) and various phospho-HSL forms (ser563, ser565, and ser660) in adipocyte-like 3T3-L1 cells expressing human stomatin, or not, were examined by Western blotting analyses. No significant difference have been observed between overexpression of stomatin and the control. **B)** Energy expenditure and **C)** thermogenesis of STOM Tg mice and WT littermate mice after 5-month high fat diet (HFD) feeding were determined. Both measurements showed no significant difference in respiratory exchange ratio (RER) and heat production comparing STOM Tg with the control. **D)** Serum triglyceride and cholesterol concentrations of STOM Tg fed with HFD for 20 weeks exhibited no significant difference comparing to the control WT littermate mice. Each dot represents one mouse. Mean ± s.d. is shown.

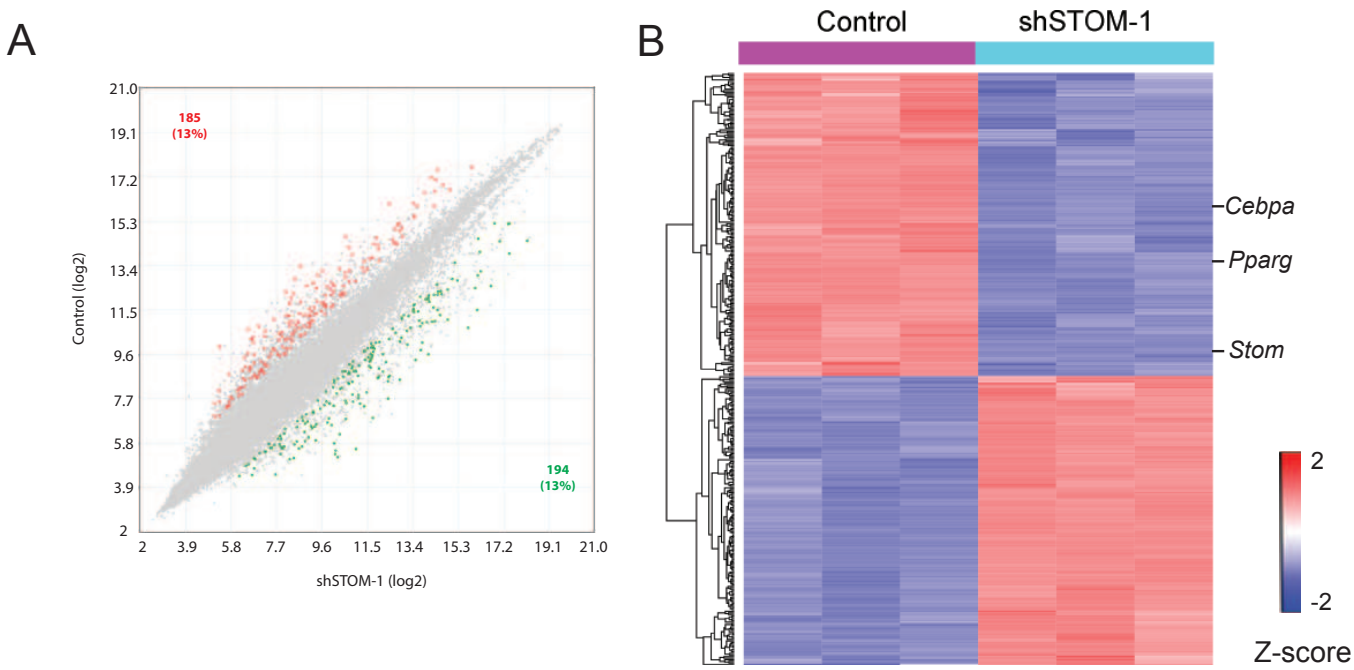

Supplemental Figure 3: Transcriptome analyses of shSTOM-1 and control cells after induction of adipogenic differentiation. A) Scatter plots of the normalized signal intensities of 1,478 genes that exhibited differential expressions between shSTOM-1 and control cells. Log2 intensities for each spot on the microarray are plotted on the x and y axes with signals from root tips stressed for control and shSTOM-1. The diagonal lines represent fold change cutoffs of ±3. The red spots represent up-regulated genes and the green spots indicate down-regulated genes. **B)** Hierarchical cluster analyses of the 1,478 genes shown in **A)**. Data were collected from three independent cell clones. Relative expression levels of genes are illustrated by the color gradient (Z-score).

Figures

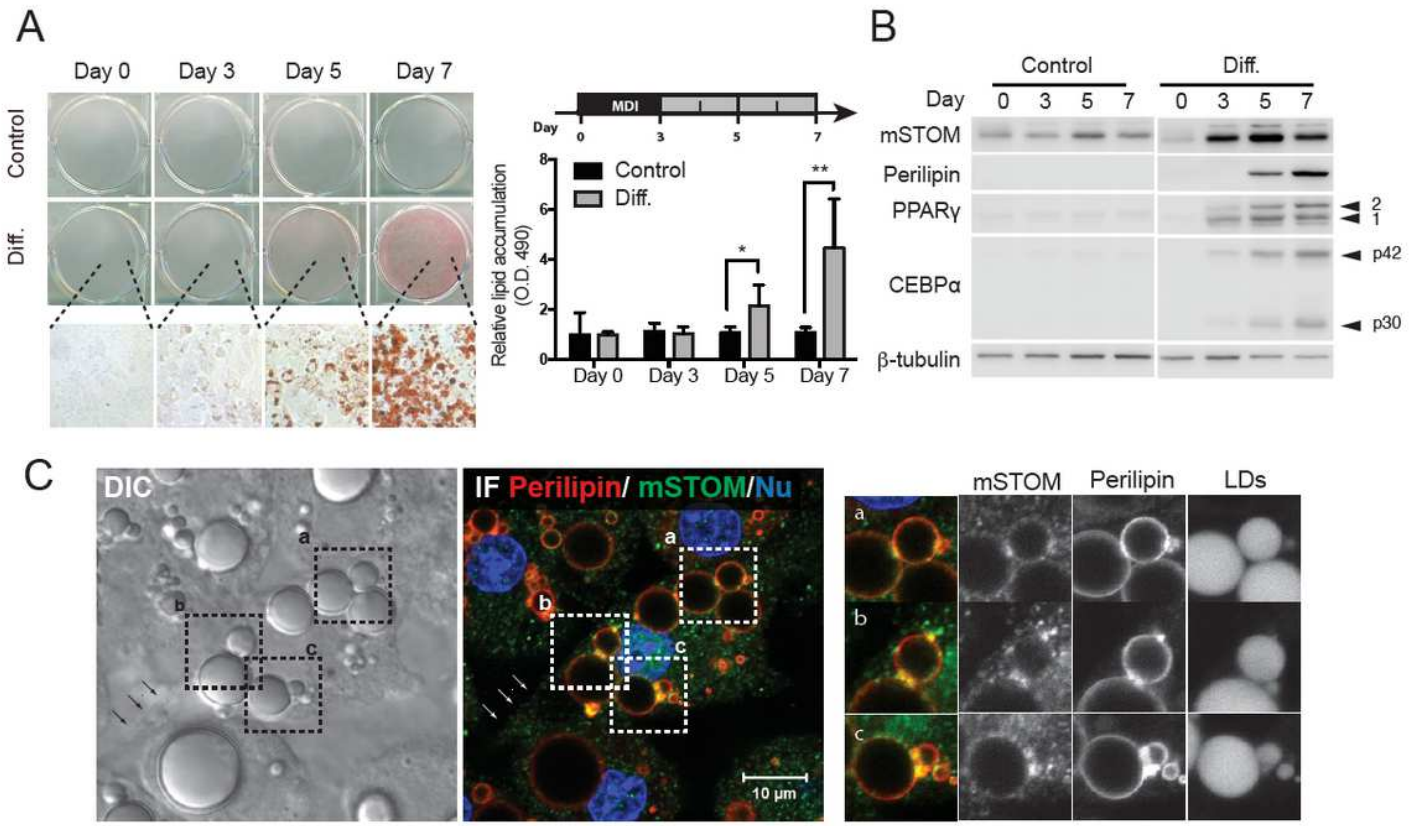

Figure 1

Stomatin expressions increased during adipogenesis. A) Mouse 3T3-L1 fibroblasts were treated with MDI induction medium (Diff.) or control vehicle. On day 0, 3, 5, 7 after induction, cells were stained with Oil Red O and observed under microscopy. The amounts of lipid accumulation for individual culture plates were quantified by measuring absorbance at 490 nm (OD 490). Mean ± s.d. for six independent experiments. **P<0.01 and ****P<0.0001 by two-way ANOVA analysis. B) On the day after induction as indicated, Western blotting analyses revealed increased expressions of mouse stomatin (mSTOM), perilipin, PPARγ and C/EBPα. C) Subcellular distributions of endogenous stomatin (green) and perilipin (red) on cells after 7-day induction were observed by DIC and immunofluorescence microscopy (IF). Cell nuclei were revealed by DNA stain (blue). Perilipin and mSTOM were found colocalized on vesicular membranes of lipid droplets (LDs) (inset). Bar = 10 μm.

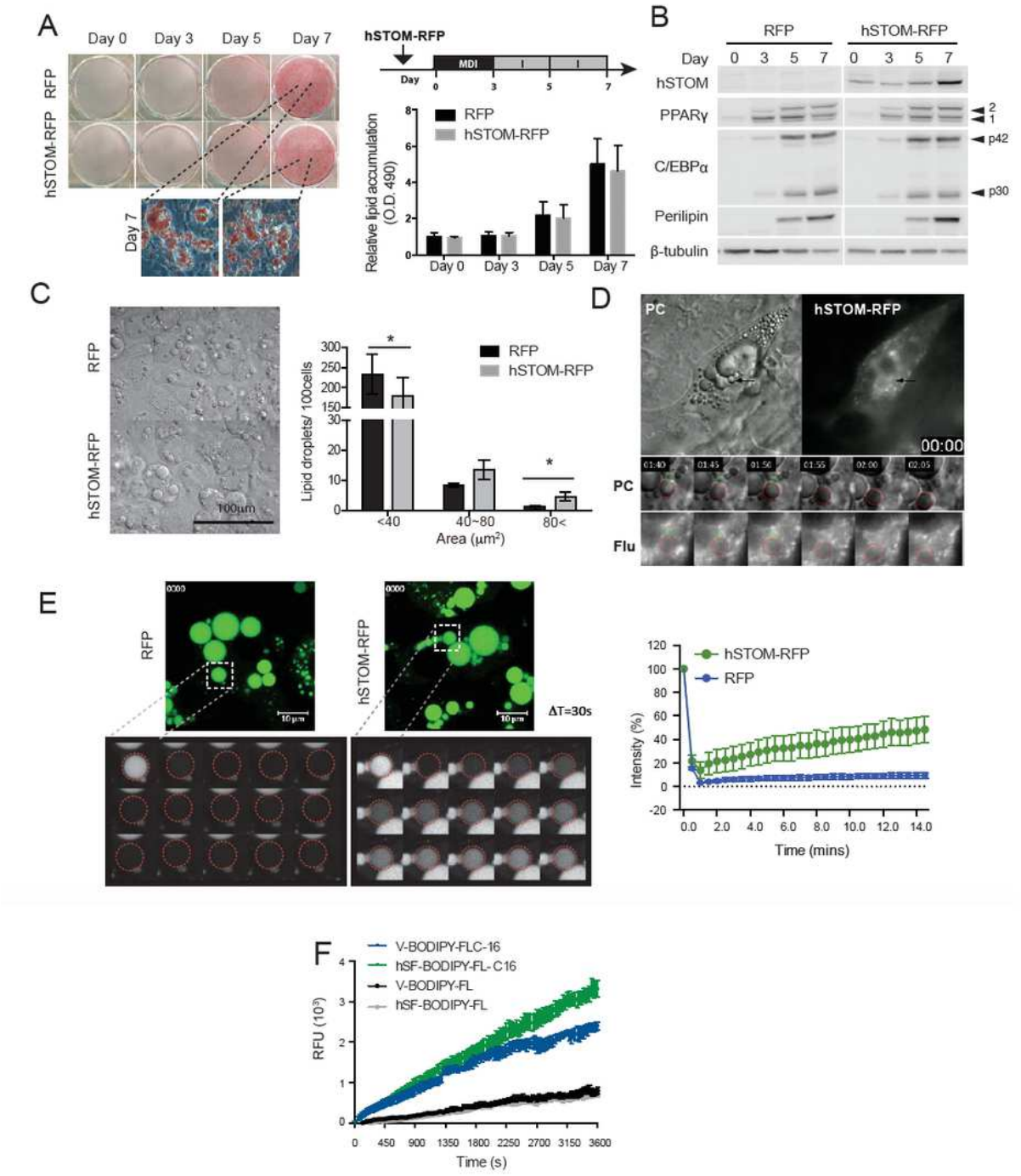

Figure 2

Overexpression of stomatin promoted lipid droplet growth and facilitated fatty acid uptake in adipocyte-like cells. A) Mouse 3T3-L1 cells over-expressing exogenous human stomatin conjugated with RFP (hSTOM-RFP) or RFP as control, were induced to differentiate into adipocyte-like cells. Lipid contents of the cells were visualized by Oil Red O staining and OD measured at 490nm. Mean ± s.d. for four independent experiments. B) Exogenous human stomatin (hSTOM), PPARγ, C/EBPα, and perilipin were

examined by Western blotting. C) The numbers and sizes of lipid droplets (LDs) in adipocyte- like cells (on day 7 of induction) were quantified after AdipoRed staining and plotted as a function of LD areas. There were larger LDs (> 80 μm2) found in cells over-expressing stomatin than the control cells, which contained mostly small (< 40 μm2) LDs. Mean ± s.e.m. for three independent experiments. *P<0.05 by paired t-test. Bar = 100 μm. D) The time-lapse recording of a LD-LD fusion event (arrow) within a live adipocyte-like 3T3-L1 cell transfected with hSTOM-RFP. A small LD (green dashed circle) was noted to fuse with a large LD (red dashed circle) then disappeared. Time of image tiles is shown as hr : min. PC: phase-contrast microscopy; Flu: fluorescence microscopy. E) Fluorescence recovery after photobleaching (FRAP) experiments were done on cells expressing hSTOM-RFP (n = 7) or RFP (n = 10). Adipocyte-like cells were pre-treated with BODIPY-FL-C12 fatty acid. Photobleaching was done at a randomly selected LD (dashed box); Afterbleaching, fluorescence recovery, as % of original intensity, was recorded by time-lapse microscopy at a 30-sec interval. Mean ± s.e.m. for three independent experiments. Bar = 10 μm. F) Adipocyte-like cells expressing FLAG-conjugated human stomatin (hSF) or vector control (V) were treated with 0.2 μM fluorescently-labeled fatty acid (BODIPY-FL-C16) to measure uptake of extracellular fatty acid into the cells, or with fluorescent tag (BODIPY-FL) as a control to measure non-specific leak of BODIPY-FL into the cell. Intracellular accumulations of fluorescence over time were recorded and plotted as a function of time. Mean ± s.e.m. for three independent experiments.

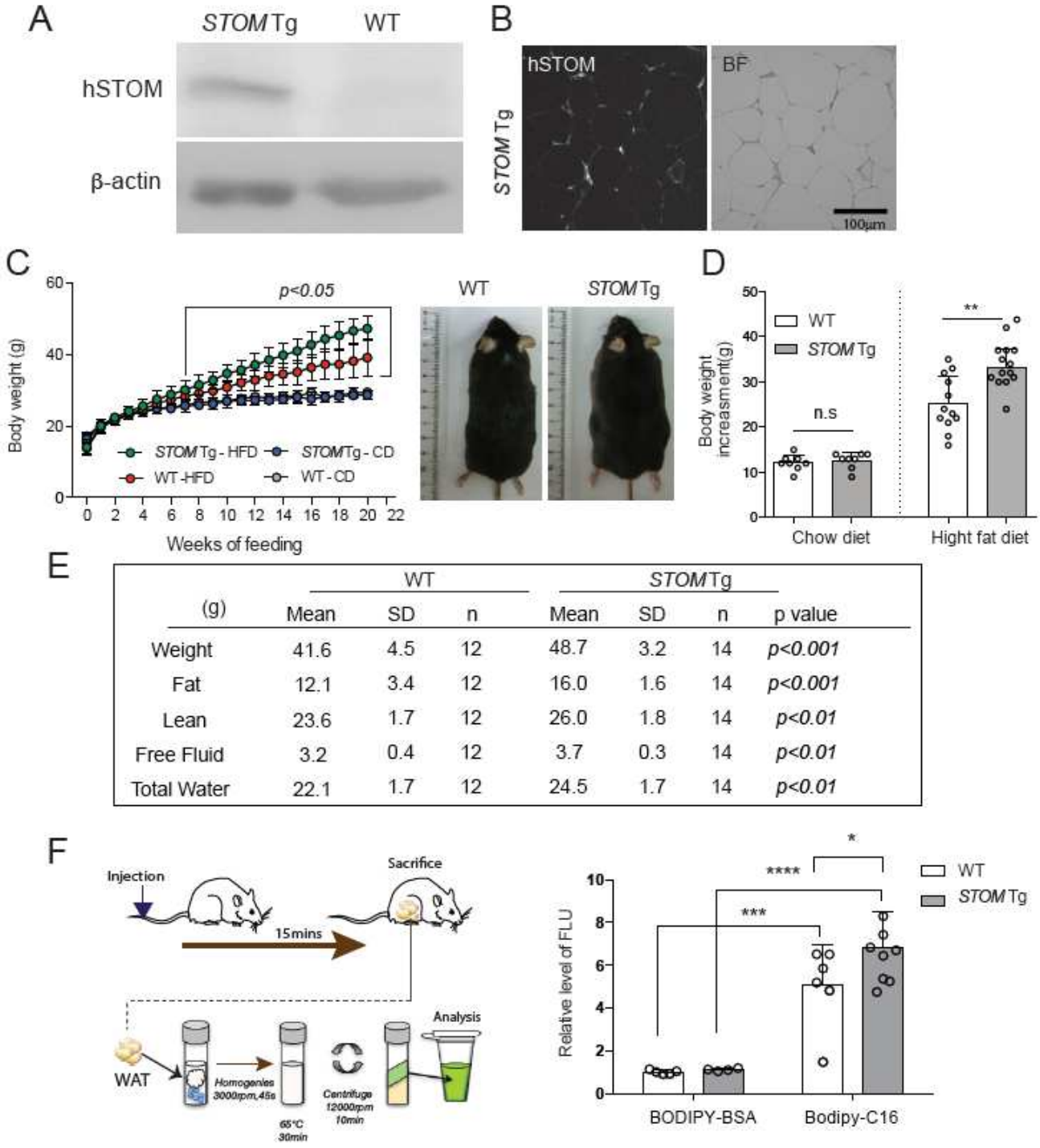

(g)	WT			STOM Tg			
	Mean	SD	n	Mean	SD	n	p value
Weight	41.6	4.5	12	48.7	3.2	14	*p<0.001*
Fat	12.1	3.4	12	16.0	1.6	14	*p<0.001*
Lean	23.6	1.7	12	26.0	1.8	14	*p<0.01*
Free Fluid	3.2	0.4	12	3.7	0.3	14	*p<0.01*
Total Water	22.1	1.7	12	24.5	1.7	14	*p<0.01*

Figure 3

Stomatin transgenic mice fed with high-fat diet were more obese than the control mice. A) Western blotting revealed high expression of human stomatin (hSTOM) in stomatin transgenic mice (STOM Tg). B) The exogenous hSTOM proteins were present mainly on surface of the adipocyte plasma membrane in fat tissues of STOM Tg mice. C) Body weight changes of STOM Tg and wild type (WT) mice fed with regular chow diet (CD) or high-fat diet (HFD) for 20 weeks. Representative photos of the mice are shown. D) Body weight increments after 20-week feeding were measured. Each dot represents one mouse. While

no difference was noticed in animals fed with CD, body weight gains were significantly higher in HFD-fed STOM Tg, compared with HFD-fed WT mice. Mean ± s.d. is shown. n.s = non-significant. **P<0.01 by unpaired t-test. E) The mass of whole body, fat, lean, free fluid, and total water were calculated for HFD-fed STOM Tg and HFD-fed WT mice. F) Fatty acid uptake was measured in vivo. Fluorescently-labeled BODIPY-FL-C16 fatty acid, or BODIPY-BSA, were injected into tail vein of STOM Tg mice or WT mice. After 15 min, aqueous portions of white adipose tissue (WAT) from the animal were extracted and fluorescence signals that represented lipid uptake were quantified. Data shown are fold changes of fluorescence intensity using BODIPY-BSA injected to WT mice as the reference. Each dot represents one mouse. Mean ± s.d. for three independent experiments. *P<0.05, **P<0.01, and ****P<0.0001 by two-way ANOVA. BODIPY-FL-C16: 4,4-Difluoro-5,7-Dimethyl-4-Bora-3a,4a-Diaza-s-Indacene-3-Hexadecanoic Acid; BSA: bovine serum albumin

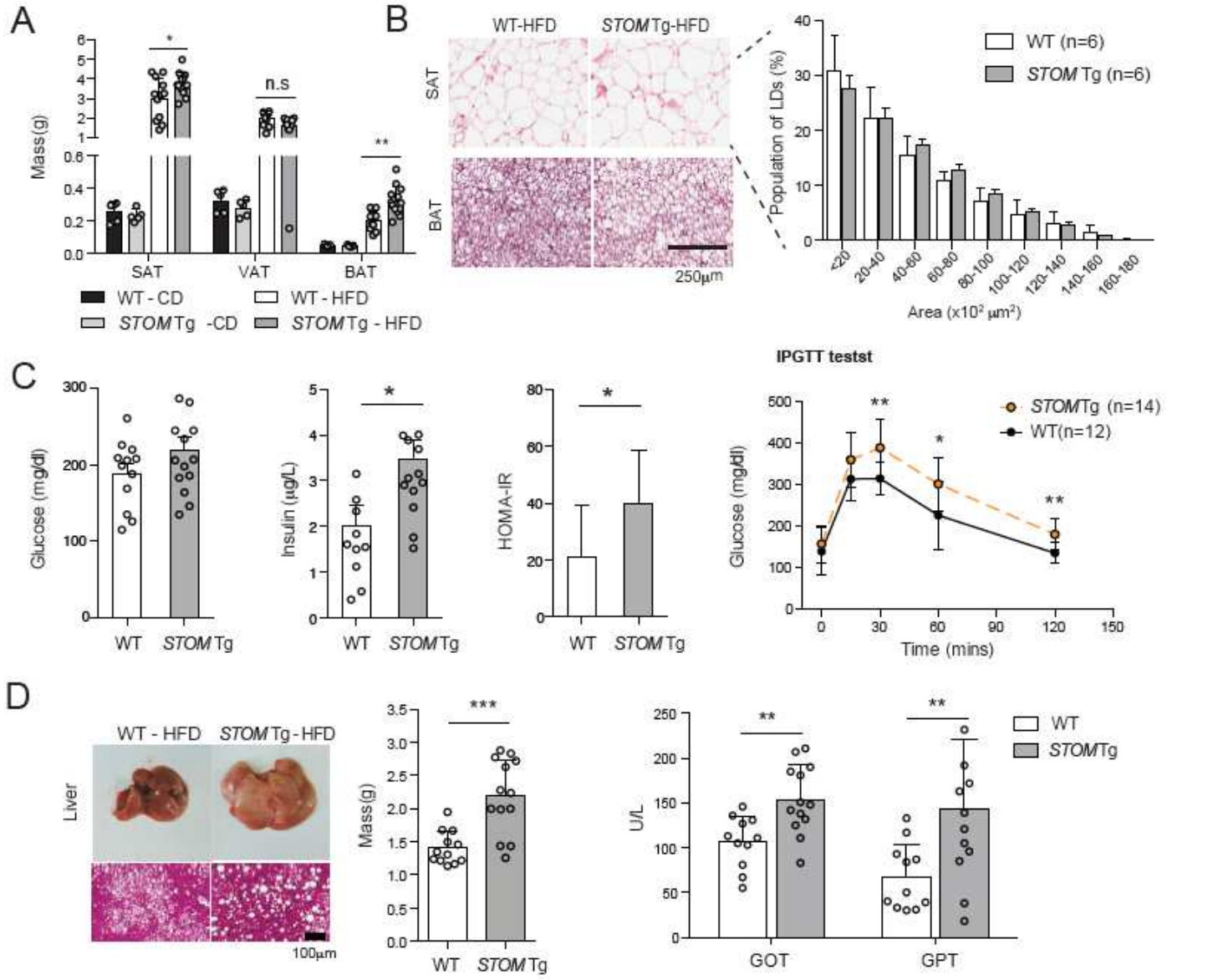

Figure 4

Stomatin transgenic mice fed with high-fat diet exhibited adipocyte hypertrophy and metabolism disorders. A) The weights of subcutaneous adipose tissue (SAT), visceral adipose tissue (VAT) and brown adipose tissue (BAT) in stomatin transgenic mice (STOM Tg) or wild type mice (WT) fed with regular chow diet (CD) or high-fat diet (HFD) for 20 weeks were measured. B) Representative H&E stained histopathological sections of SAT, and BAT from HFD-fed STOM Tg or HFD-fed WT mice. Histogram analyses of sizes of adipocytes are shown. Bar = 250μm. C) After HFD-feeding for 20 weeks, the animal's fasting glucose, serum insulin, homeostatic model assessment of insulin resistance (HOMA-IR), and intraperitoneal glucose tolerance test (IPGTT) were examined. D) The mass of liver of STOM Tg or WT mice, fed with HFD for 20 weeks, were weighed. Fatty liver changes revealed by histopathological sections and high level of serum glutamate oxaloacetate transaminase (GOT) and glutamate pyruvate transaminase (GPT) indicated impaired hepatic functions in STOM Tg mice, compared to WT mice. Bar = 100μm. Each dot represents one mouse. Mean ± s.d. is shown. n.s = non-significant. *P<0.05, **P<0.01, and ***P<0.001 by unpaired t-test.

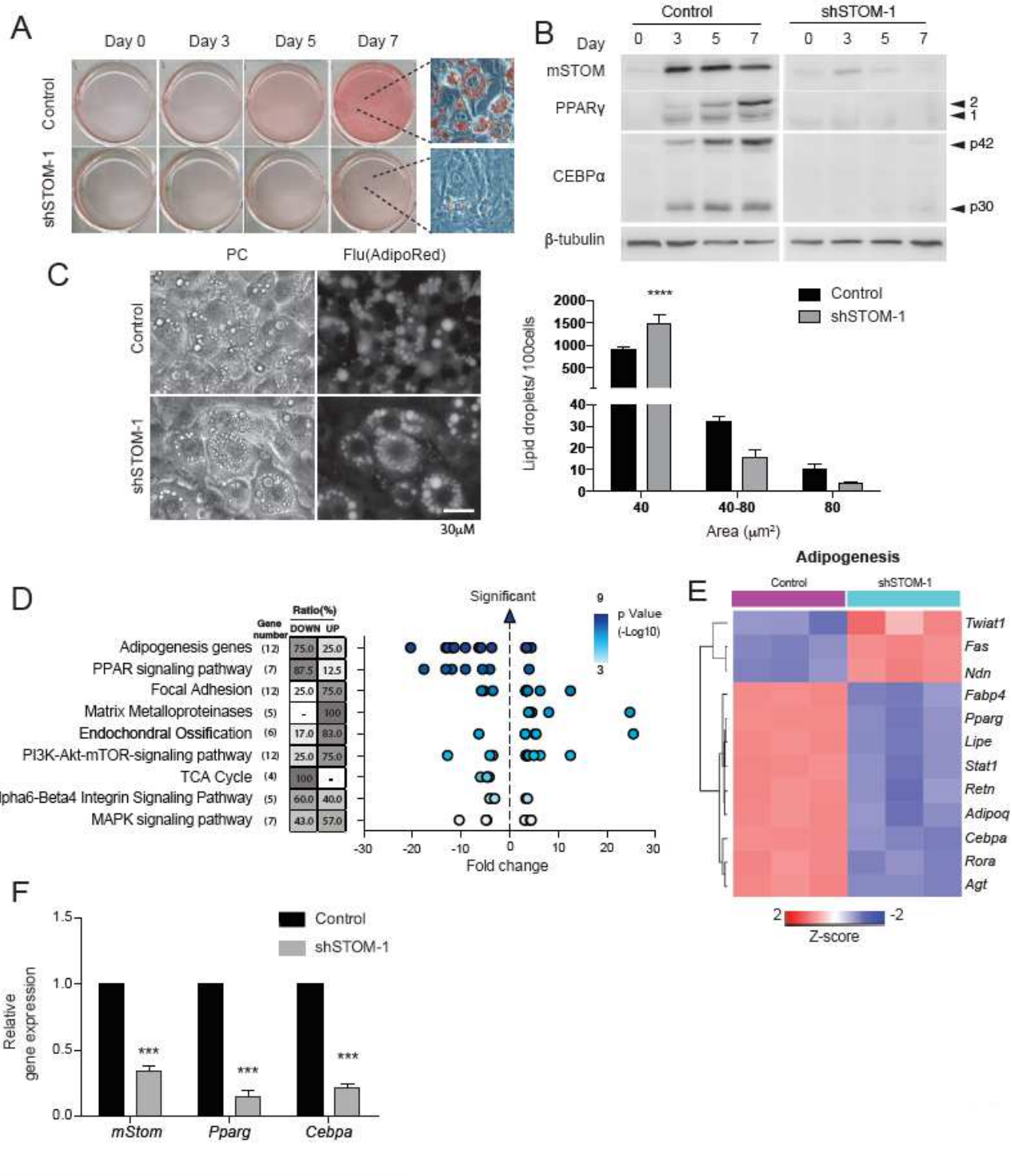

Figure 5

Decreased stomatin expression affected adipogenesis and inhibited lipid droplet growth. A) Stomatin knockdown was done by transduction of shRNA of Stomatin gene into 3T3-L1 cells generating shSTOM-1 cells or shSTOM-2 cells. After induction of adipogenic differentiation, shSTOM-1 and control cells were stained with Oil Red O. Cells after 7-day induction are shown using high-power microscopy. B) On the day after induction as indicated, Western blotting analyses revealed decreased expression of mouse stomatin

(mSTOM) by knockdown. Adipogenic proteins, including PPARγ, and C/EBPα were also down-regulated. C) On day 7 of adipogenic differentiation, adipocyte-like shSTOM-1 cells were stained with AdipoRed and observed under phase-contrast (PC) and fluorescence (Flu) microscopy. The size of lipid droplets (LDs) were measured, and their number per 100 adipocytes were calculated. Histogram analyses showed more small LDs (< 40 μm2) and fewer large (> 80 μm2) LDs in shSTOM-1 cells than the control. Mean ± s.d. for three independent experiments. ****P<0.0001 by two-way ANOVA. Bar = 30 μm. D) Transcriptome analyses of adipocyte-like shSTOM-1 and control cells after induction for 7 days. From the data of microarray assays, scatter plots revealed enriched Wiki pathways in shSTOM-1 cells comparing to the control. For a given pathway, ratio of gene number being up- or down-regulated in that pathway were determined, and plotted as function of fold change. Each dot represents one gene. The color of the dots represents the range of P-values related to the indicated pathway. E) Heat map of adipogenesis gene obtained from the enrichment-based cluster analysis of the Wiki pathway. F) Real-time qPCR analyses to validate the changed genes revealed by microarray assays. Data shown are fold changes relative to Nono mRNA level. Mean ± s.d. for three independent experiments. ***P<0.001 by unpaired t-test.

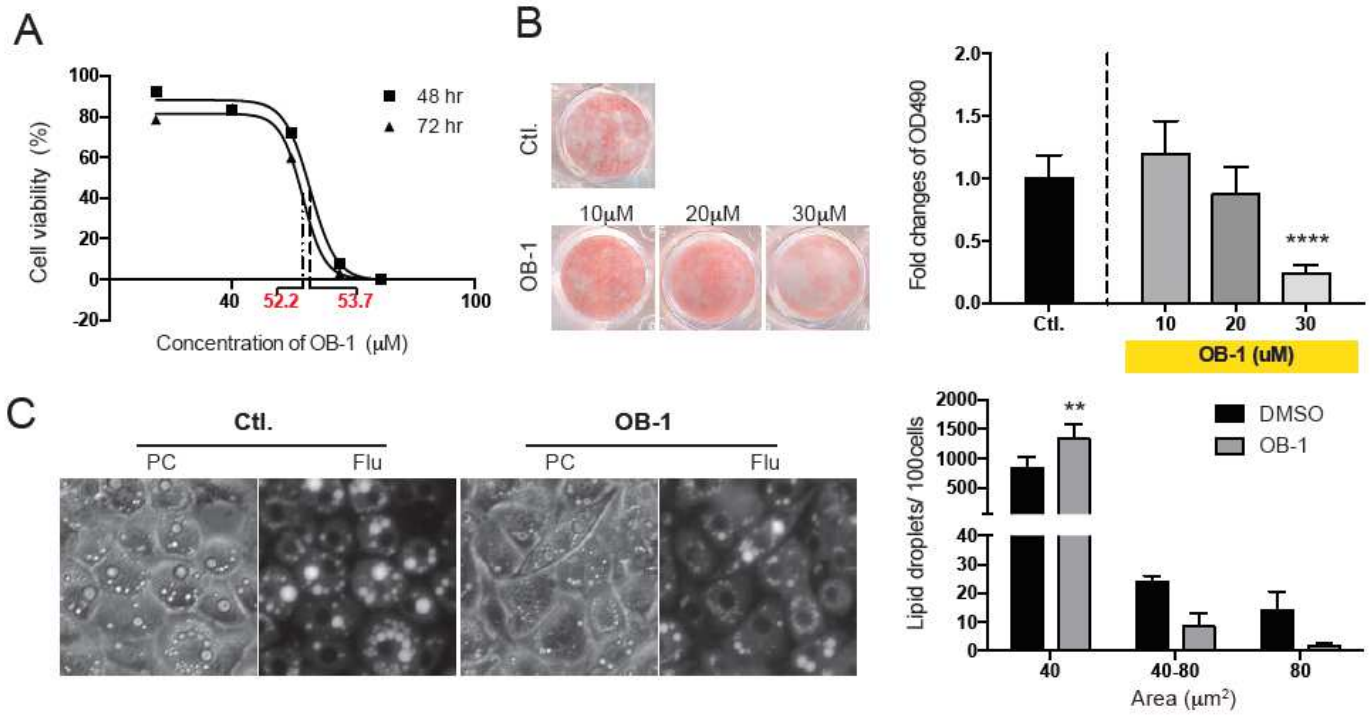

Figure 6

Stomatin inhibitor OB-1 inhibited adipogenesis and hindered lipid droplet growth. A) Cell viability after OB-1 treatments for 48h or 72h were tested by MTT assays. LC50 of OB-1 were calculated from three independent experiments. B) Culture adipocyte-like 3T3-L1 plates treated with or without OB-1 at concentrations indicated, were stained with Oil Red O and subjected to OD 490 quantifications. Note OB-1 inhibited adipogenesis in a dose-dependent manner, compared to the control DMSO treatment. Each OB-1 treatment data was normalized to the corresponding DMSO vehicle control; fold changes are shown. Mean ± s.d. for three independent experiments (n=9 for each experiment). ****P<0.0001 by one-way

ANOVA. C) Adipocyte-like 3T3-L13T3-L1 cells after 7-day induction were treated with 25μM OB-1 or control vehicle, and stained with AdipoRed. The cells were observed under phase contrast (PC) or fluorescence microscopy (Flu) to determine the numbers and sizes of LD. Histogram analyses showed increased small LDs (< 40 μm2) and decreased large (> 80 μm2) LDs after OB-1 treatments, compared to the control. Mean ± s.d. for three independent experiments. **P<0.01 by two-way ANOVA. Bar = 30 μm.

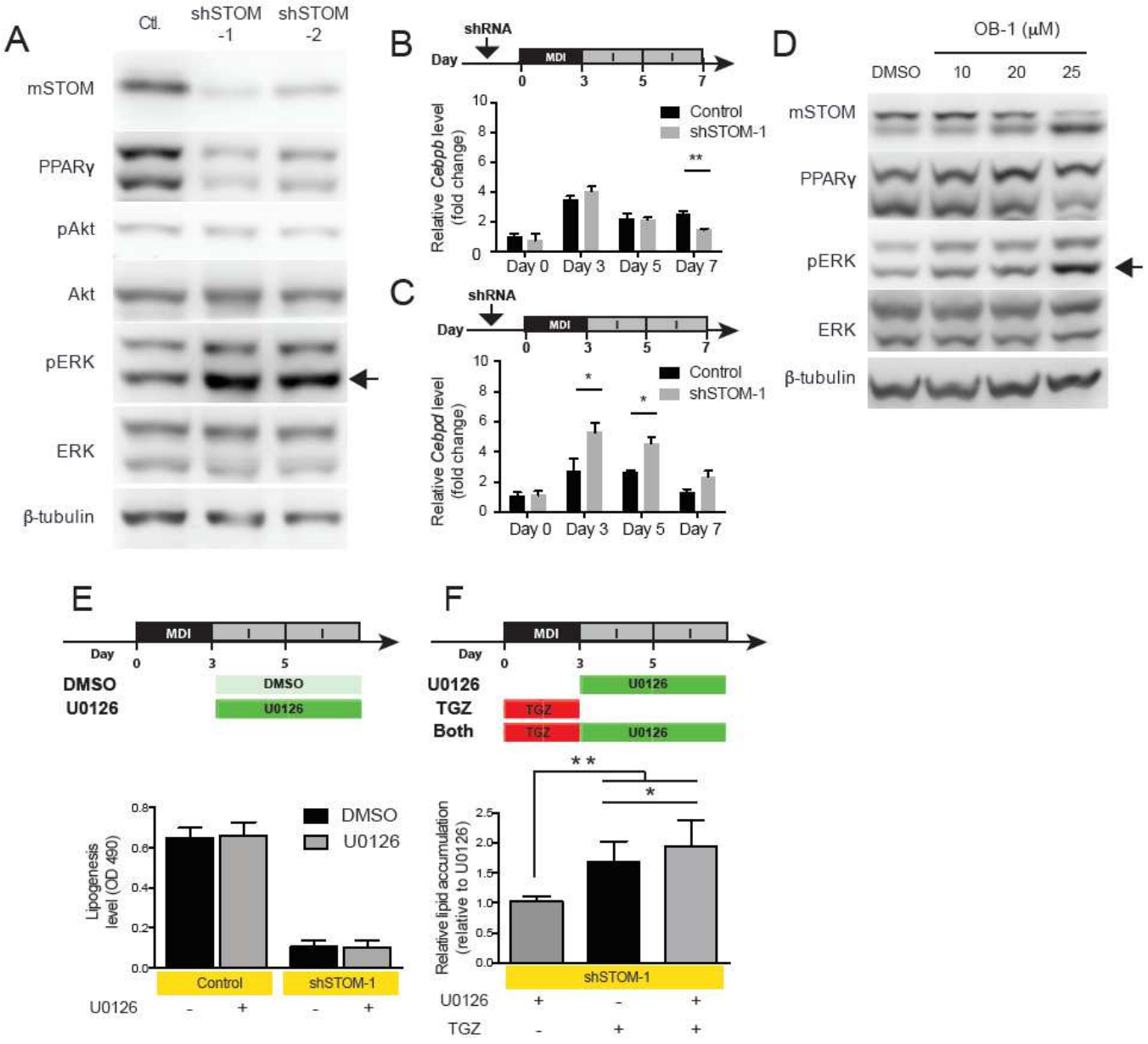

Figure 7

Knockdown of stomatin activated ERK-pathway. A) shRNA were transducted into 3T3-L1 cells to knockdown stomatin and generating shSTOM-1 and shSTOM-2 cells. After induction of differentiation, Western blotting analyses were done. Although Akt pathway remained unchanged, the ERK pathway was activated as evidenced by increased pERK (arrow). B, C) Expressions of early adipogenic genes, Cebpb and Cebpd, were examined at mRNA level by qPCR. B) Expressions of Cebpb increased in the first three days of adipogenic differentiation, and subsequently decreased. Knockdown of stomatin (exemplified by

shSTOM-1 cells) did not significantly influence this pattern. C) Expressions of Cebpd gene also exhibited a transient early increase then declined; however, knockdown of stomatin appeared to significantly increase and maintain Cebpd expression at a relatively higher level than the control. The house-keeping Nono gene was used as the reference for qPCR exoeriments. *P<0.05 by unpaired t-test. D) Treating adipocyte-like cells with stomatin inhibitor OB-1 also resulted in activation of ERK pathway, evidenced by increased pERK (arrow). E) Levels of lipogenesis by adipocyte-like 3T3-L1 cells were quantified by measuring OD 490 after Oil Red O staining. Treating shSTOM-1 cells with 10μM U0126, an ERK pathway inhibitor, from day3 to day 7, did not reverse the lipogenesis inhibition caused by stomatin knockdown. F) On the other hand, treating shSTOM-1cells with TGZ, a PPARγ activator, in the first three days of adipogenic differentiation, was able to partially recover the knockdown-caused lipogenesis deficit; treating shSTOM-1cells with both TGZ and U0126 was noted to further increase lipid accumulation. Mean ± s.d. for six independent experiments. *P<0.05, and **P<0.01 by one-way ANOVA. qPCR: quantitative real-time PCR.

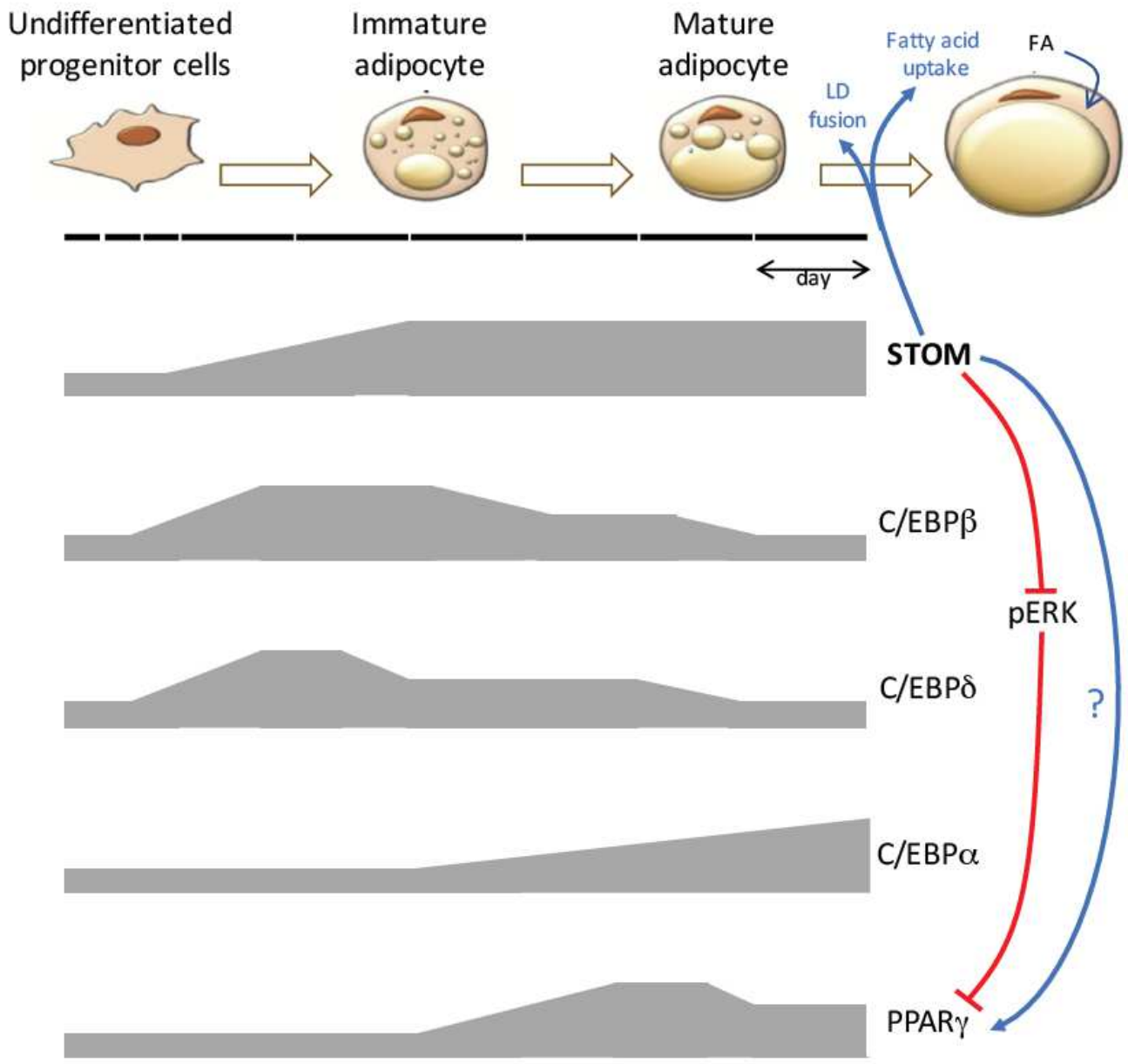

Figure 8

Stomatin's roles in modulating adipogenic differentiation and lipogenesis. Undifferentiated progenitor cells can be induced to undergo adipogenic differentiation to become immature adipocytes, and further develop into mature adipocytes, characterized by fatty acid uptake, production of lipid, and fusions and enlargements of lipid droplets (LDs). Dynamic expressions of adipogenic genes along this process are depicted. Stomatin progressively increases during adipocyte differentiation and maturation, and participates not only in fatty acid uptake and LD fusions, but also in modulation of adipogenic gene expressions. By inhibiting pERK, stomatin activates PPARγ: resulting in adipocyte maturation and lipogenesis. Stomatin also plays a role in regulating early phase adipogenic genes, such as C/EBPβ and

C/EBPδ through currently unknown mechanisms. C/EBP: CCAAT/enhancer binding protein; PPARγ: peroxisome proliferator-activated receptor-γ.

Supplementary Files

This is a list of supplementary files associated with this preprint. Click to download.

- Supplementalvedio1LDLDfusionmovie.mp4